On the relationship between Nd isotopic composition and ocean overturning circulation in idealized freshwater discharge events

Johannes Rempfer,[1,2] Thomas F. Stocker,[1,2] Fortunat Joos,[1,2] and Jean-Claude Dutay[3]

Received 2 March 2012; revised 19 June 2012; accepted 20 June 2012; published 9 August 2012.

[1] Using a cost-efficient climate model, the effect of changes in overturning circulation on neodymium isotopic composition, ϵ_{Nd}, is systematically examined for the first time. Idealized sequences of abrupt climate changes are induced by the application of periodic freshwater fluxes to the North Atlantic (NA) and the Southern Ocean (SO), thus mainly affecting either the formation of North Atlantic Deep Water (NADW) or Antarctic Bottom Water (AABW). Variations in ϵ_{Nd} reflect weakening and strengthening of the formation of NADW and AABW, changes in ϵ_{Nd} of end-members are relatively small. Relationships between ϵ_{Nd} and the strength of NADW or AABW are more pronounced for AABW than for NADW. Atlantic patterns of variations in ϵ_{Nd} systematically differ between NA and SO experiments. Additionally, the signature of changes in ϵ_{Nd} in the Atlantic and the Pacific is alike in NA but opposite in SO experiments. Discrimination between NA and SO experiments is therefore possible based on the Atlantic pattern of variations in ϵ_{Nd} and the contrariwise behavior of ϵ_{Nd} in the Atlantic and the Pacific. In further experiments we examined the effect of variations in magnitudes of particle export fluxes. Within the examined range, and although settling particles represent the only sink of Nd, their effects on ϵ_{Nd} are relatively small. Our results confirm the large potential of ϵ_{Nd} as a paleocirculation tracer but also indicate its limitations of quantitative reconstructions of changes in the Atlantic Meridional Ocean Circulation.

Citation: Rempfer, J., T. F. Stocker, F. Joos, and J.-C. Dutay (2012), On the relationship between Nd isotopic composition and ocean overturning circulation in idealized freshwater discharge events, *Paleoceanography*, *27*, PA3211, doi:10.1029/2012PA002312.

1. Introduction

[2] Reconstructions of past changes in ocean overturning circulation have been proposed from records of paleocirculation proxies that reflect the distribution of water masses or the rate of ocean circulation and that can be measured in sediment cores. For this reason, considerable work has been put into the investigation of the cycling of various elements, as well as elemental and isotope ratios (see *Lynch-Stieglitz* [2003] for an overview). However, an unequivocal reconstruction of changes in past overturning circulation is difficult, and still not even possible for the Last Glacial Maximum (LGM), a period of time for which a wide range of data is available [*Lynch-Stieglitz et al.*, 2007; *Marchal and Curry*, 2008; *Hesse et al.*, 2011]. A relatively novel and promising quasi-conservative tracer of water mass distribution and mixing is the isotopic composition of neodymium (ϵ_{Nd}) [*von Blanckenburg*, 1999; *Burton and Vance*, 2000; *Frank*, 2002].

[3] The purpose of this study is to systematically examine the effect of changes in overturning circulation on ϵ_{Nd} in idealized sequences of abrupt climate change for the first time. The timing of the sequences is chosen to shed some light on the characteristics of ϵ_{Nd} expected during Heinrich and Dansgaard-Oeschger (DO) events. This may contribute to a better knowledge of the effects of changes in the strength of the ocean overturning circulation of different magnitude and duration on ϵ_{Nd}.

[4] The Nd isotopic ratio ($^{143}Nd/^{144}Nd$) of a sample relative to the "bulk earth" standard value of 0.512638 [*Jacobsen and Wasserburg*, 1980] is reported as

$$\epsilon_{Nd} = \left(\frac{\left(^{143}Nd/^{144}Nd\right)_{sample}}{\left(^{143}Nd/^{144}Nd\right)_{std}} - 1 \right) \cdot 10^4. \qquad (1)$$

Isotopes ^{143}Nd and ^{144}Nd have recently been included into a cost-efficient, dynamical ocean model of intermediate complexity and are simulated in reasonable agreement with available observations [*Rempfer et al.*, 2011].

[1]Climate and Environmental Physics, Physics Institute, University of Bern, Bern, Switzerland.
[2]Oeschger Centre for Climate Change Research, University of Bern, Bern, Switzerland.
[3]Laboratoire des Sciences du Climat et de l'Environnement (LSCE), IPSL, CEA/UVSQ/CNRS, Gif sur Yvette, France.

Corresponding author: J. Rempfer, Climate and Environmental Physics, Physics Institute, University of Bern, Sidlerstr. 5, CH-3012 Bern, Switzerland. (rempfer@climate.unibe.ch)

0883-8305/12/2012PA002312

[5] Past Nd isotopic composition of deep water masses is recorded reliably in manganese nodules [*Albarède and Goldstein*, 1992; *Albarède et al.*, 1997], ferromanganese crusts [*Piepgras et al.*, 1979; *Piepgras and Wasserburg*, 1980; *Albarède and Goldstein*, 1992; *Rutberg et al.*, 2000], benthic foraminifera [*Klevenz et al.*, 2008; *Elmore et al.*, 2011], fish debris [*Martin and Haley*, 2000] and deep-sea coral aragonite [*van de Flierdt et al.*, 2010]. In recent years, millennial-scale as well as glacial-interglacial variations in ϵ_{Nd} extracted from such archives are increasingly being interpreted in terms of changes in the distribution of water masses [e.g., *Rutberg et al.*, 2000; *Piotrowski et al.*, 2004, 2005, 2008; *Gutjahr et al.*, 2008; *Piotrowski et al.*, 2009; *Robinson and van de Flierdt*, 2009; *Gutjahr et al.*, 2010; *Roberts et al.*, 2010; *Gutjahr and Lippold*, 2011].

[6] All these studies indicate the potential of ϵ_{Nd} as a complementary tracer of past water mass mixing. However, some uncertainty is associated with Nd, complicating attempts to interpret variations in ϵ_{Nd} simply due to changes in overturning circulation. First of all, considerable uncertainties are associated with the nature and magnitude of Nd-sources and sinks [e.g., *Goldstein and Jacobsen*, 1987; *Jeandel et al.*, 1995; *Tachikawa et al.*, 1999; *Frank*, 2002; *Tachikawa et al.*, 2003; *van de Flierdt et al.*, 2004; *Lacan and Jeandel*, 2005a; *van de Flierdt et al.*, 2007; *Arsouze et al.*, 2007; *Siddall et al.*, 2008; *Arsouze et al.*, 2009; *Rempfer et al.*, 2011]. Though, an adequate representation of Nd sources and sinks is an important prerequisite for the simulation of present-day observations of dissolved Nd concentrations and ϵ_{Nd} [*Rempfer et al.*, 2011]. In addition, *Tachikawa et al.* [2003] indicated that changes in the magnitude and ϵ_{Nd} of Nd sources over the years potentially affect ϵ_{Nd} of deep water masses besides changes in water mass mixing. Naturally, the extent of such changes is difficult to constrain. J. Rempfer et al. (Sensitivity of Nd isotopic composition in seawater to changes in Nd sources and paleoceanographic implications, submitted to *Journal of Geophysical Research*, 2012) reconsidered these concerns and found that rather extreme changes in magnitude and ϵ_{Nd} in Nd sources are necessary to cause a magnitude in variations in ϵ_{Nd} as observed, e.g., on glacial-interglacial time-scales. Furthermore, the interpretation of variations in reconstructed ϵ_{Nd} as changes in overturning circulation relies on the assumption that changes in the end-member composition can be neglected. Indeed, ϵ_{Nd} in the North Atlantic seems to have been relatively stable during parts of the last 30 kyr [*van de Flierdt et al.*, 2006] and during the last 5 glacial cycles [*Foster et al.*, 2007], respectively. However, these studies were either restricted to short time periods [*van de Flierdt et al.*, 2006] or rely on data with relatively low temporal resolution [*Foster et al.*, 2007]. Moreover, *Gutjahr et al.* [2008] and *Arsouze et al.* [2008] indicated that during the LGM ϵ_{Nd} of North Atlantic Deep Water (NADW, i.e., of Glacial North Atlantic Intermediate Water, GNAIW) may have been different. Finally, the paleoceanographic potential of ϵ_{Nd} has not been examined in a comprehensive way in modeling studies, as these were restricted either by computational costs or by the chosen approach. That is, to date only one modeling study is available that is based on a relatively simple approach of restoring ϵ_{Nd} at the continental margins [*Arsouze et al.*, 2008]. This study aimed to examine the effects of changes in Meridional Overturning Circulation (MOC) during the LGM on ϵ_{Nd}.

[7] Our comprehensive approach together with the high computational efficiency of the Bern3D model allows us to examine the paleoceanographic potential of ϵ_{Nd} in a systematic way and it will therefore contribute to the interpretation of variations in reconstructed ϵ_{Nd} as past changes in overturning circulation.

[8] In order to examine the sensitivity of ϵ_{Nd} in seawater to transient changes in overturning circulation, different periods and amplitudes of the forcing are investigated (section 4). Besides, we evaluate potential effects of variations in particle fluxes on variations in ϵ_{Nd} (section 5). Further information that may be derived from variations in ϵ_{Nd} in sediment cores, such as changes in the rate and the origin of changes in the overturning circulation, is discussed in section 6. Finally, we summarize our findings and draw some conclusions regarding the paleoceanographic potential of ϵ_{Nd} (section 7).

2. Methods

[9] For our simulations we use the Bern3D ocean model of intermediate complexity [*Müller et al.*, 2006], coupled to an energy balance model [*Ritz et al.*, 2011a, 2011b]. The ocean model is based on the three-dimensional frictional geostrophic balance model of *Edwards and Marsh* [2005]. Resolution in the horizontal is 36 × 36 grid cells, equidistant in longitude and in the sine of latitude. Spacing of the 32 depth layers is logarithmic, i.e., the thickness increases with depth from 39 m in the uppermost to 397 m in the bottom layer. The Bern3D model is computationally very efficient and thus well suited for long-term paleoclimate simulations [*Ritz et al.*, 2011a] as well as for sensitivity studies [e.g., *Tschumi et al.*, 2008; *Parekh et al.*, 2008; *Rempfer et al.*, 2011; *Ritz et al.*, 2011b]. The model contains a biogeochemical module, in which particle export fluxes of calcite ($CaCO_3$), opal, and Particulate Organic Carbon (POC) are calculated from prognostic equations using P, Si, and Fe as limiting nutrients (see *Parekh et al.* [2008] and *Tschumi et al.* [2008] for a detailed description). Neodymium isotopes ^{143}Nd and ^{144}Nd, which we are focusing on in this study, have recently been included, and a detailed description of the approach is given in a previous study [*Rempfer et al.*, 2011]. Since the publication of this study, an error was found in the module which affected the calculation of the global mean concentration of $CaCO_3$, opal, and POC (indicated in *Rempfer et al.* [2011, Table 2]). This error however does not affect the main conclusions of *Rempfer et al.* [2011]. Updated values of global mean particle concentrations are $3.3 \cdot 10^{-6}$ kg m^{-3} for POC, $1.6 \cdot 10^{-6}$ kg m^{-3} for $CaCO_3$, and $5.9 \cdot 10^{-6}$ kg m^{-3} for opal. For the purpose of this study we couple the ocean model to an energy-moisture balance model permitting transient simulations. Resulting annual mean Atlantic Meridional Overturning Circulation (AMOC), Pacific Meridional Overturning Circulation (PMOC) and global MOC are shown in Figure 1. Note that the wind-driven mixed layer, i.e., depths shallower than 400 m, is not taken into account for the calculation of AMOC, PMOC, and global MOC. Furthermore, note that in the following the minimum of the global MOC, i.e., deep overturning in the Southern Ocean (SOMOC), is referred to as ψ_{SOMOC}. In this set up simulated pattern and

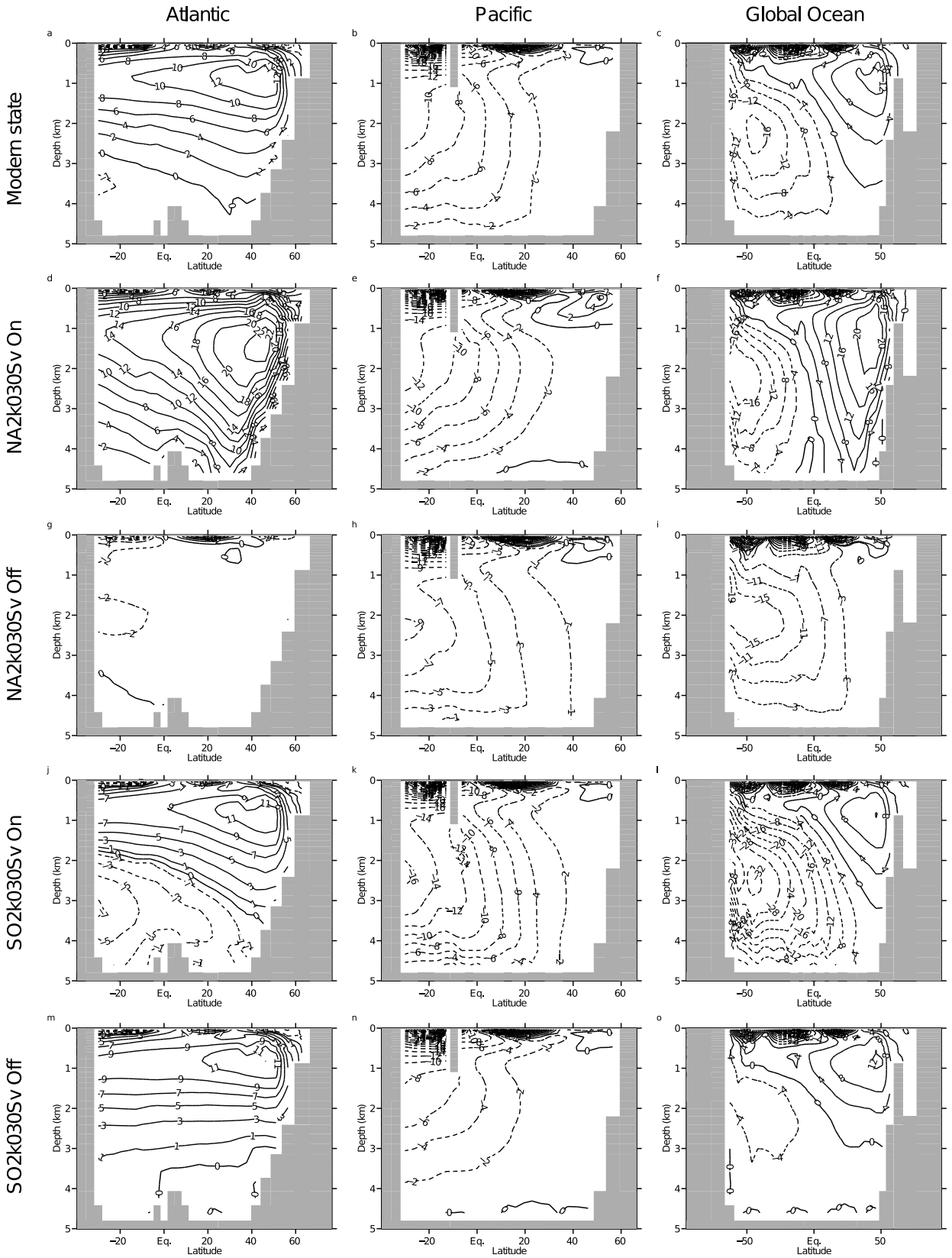

Figure 1. Annual mean meridional overturning circulation in the Atlantic, the Pacific and the Global ocean for (a–c) the CTRL, as well as for on- and off-states for experiments (d–i) NA2k030Sv and (j–o) SO2k030Sv (see Table 2 for further details). Solid lines indicate positive (clockwise) circulation, dashed lines indicate negative (counterclockwise) circulation. Contour interval is 2 *Sv* (10^6 m^3 s^{-1}) in Atlantic and Pacific, and 4 *Sv* in the Global ocean cases, respectively.

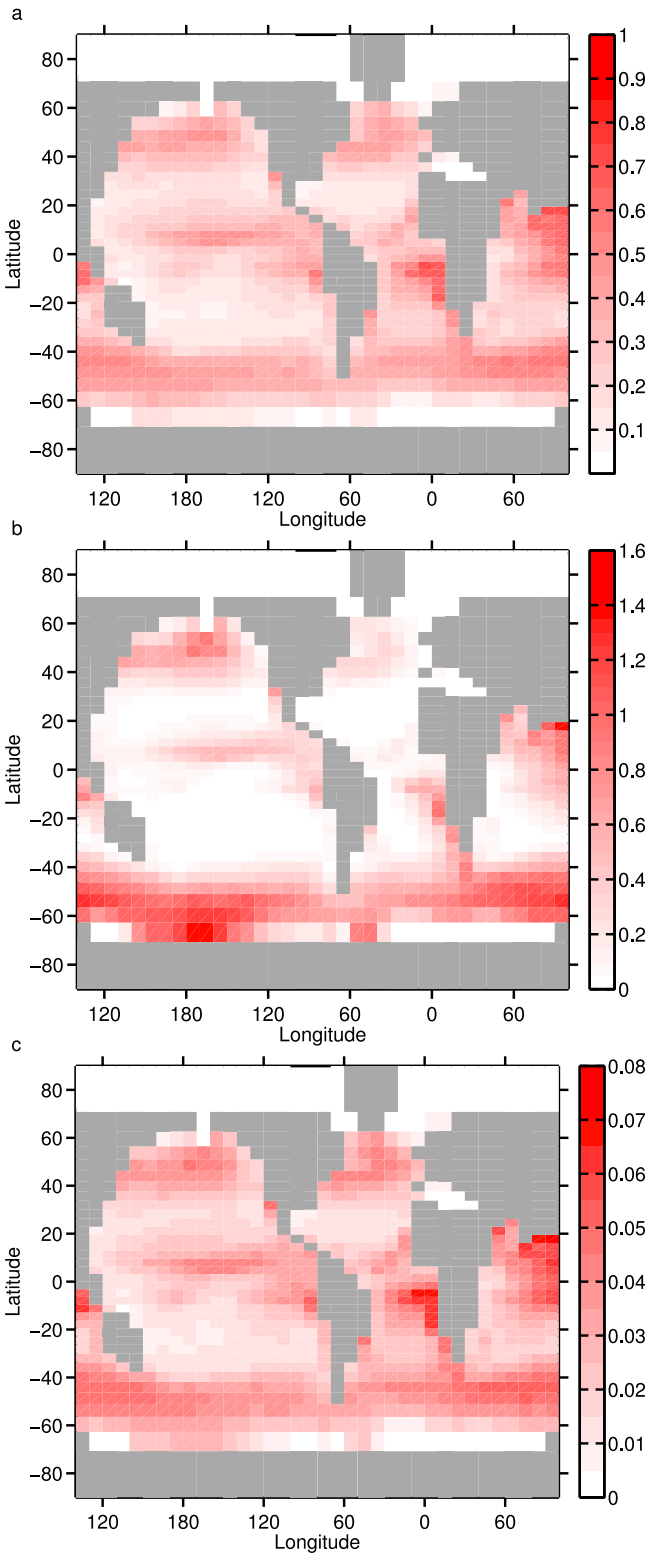

Figure 2. Global maps of steady state export production of (a) $CaCO_3$ (mol C m^{-2} yr^{-1}), (b) opal (mol Si m^{-2} yr^{-1}), and (c) POC (mol C m^{-2} yr^{-1}). Globally integrated fluxes are 1.16 Gt C yr^{-1}, 101 Tmol Si yr^{-1}), and 13 Gt C yr^{-1}, respectively, and are comparable to available estimates [*Sarmiento and Gruber*, 2006].

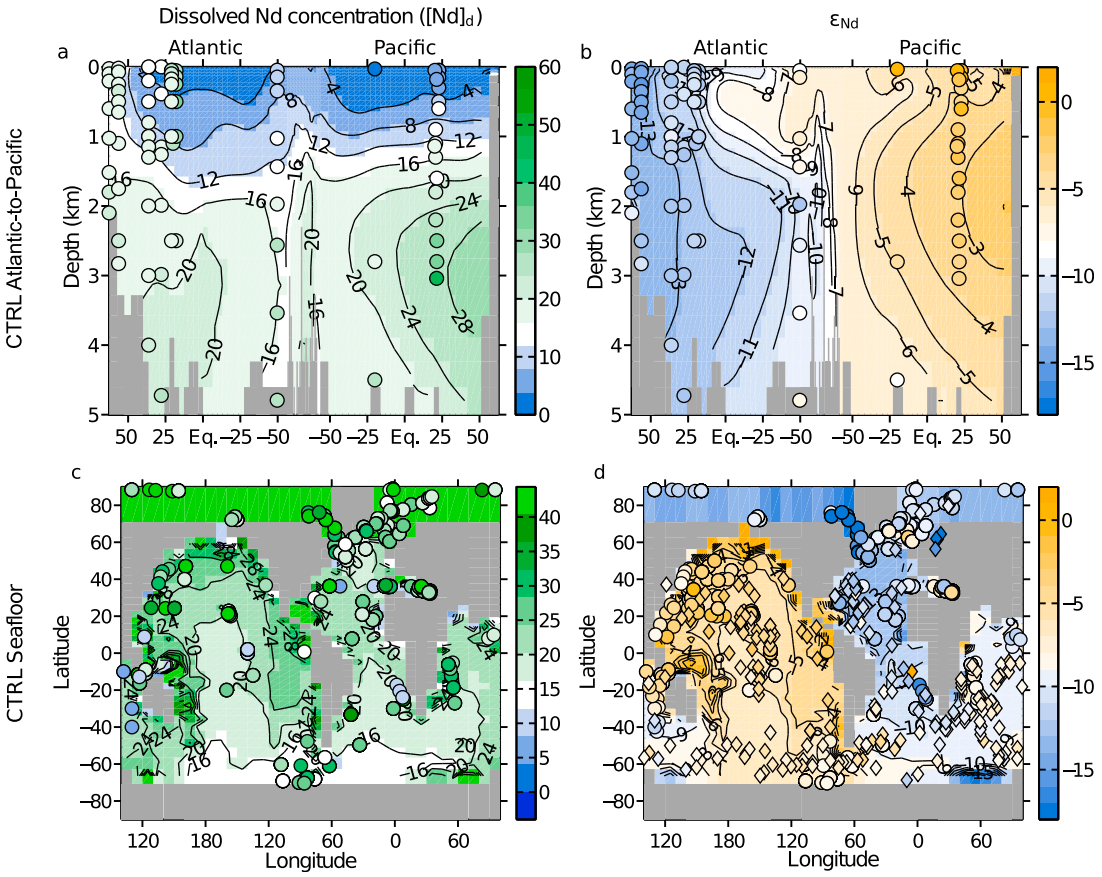

Figure 3. (a, c) $[Nd]_d$ (pmol kg^{-1}) and (b, d) ϵ_{Nd} obtained with the CTRL, in vertical sections (top) along a track from the Atlantic to the Pacific (the course of the track is indicated in *Rempfer et al.* [2011, Figure 1a]) and (bottom) at the seafloor. Observations are superimposed as colored circles, using the same color scale (references are given in section 2). Concentrations up to 28 pmol kg^{-1} are indicated as contours at an interval of 4 pmol kg^{-1}.

strength of the meridional overturning circulation (Figures 1a–1c) as well as patterns and magnitude of particle export fields of $CaCO_3$, opal and POC (Figure 2) slightly differ from those in *Rempfer et al.* [2011]. As changes in overturning and in particle export fields affect the efficiency and the spatial pattern of the sink of Nd it was necessary to retune the Nd-module. We therefore repeated the calibration procedure of *Rempfer et al.* [2011] and minimized cost-functions for dissolved Nd concentration ($[Nd]_d$) as well as ϵ_{Nd} (not shown). A recent compilation of observations of $[Nd]_d$ and ϵ_{Nd} by Francois Lacan was downloaded from the Internet (http://www.legos.obs-mip.fr/fr/equipes/geomar/results/database_may06.xls). The compilation includes observations of $[Nd]_d$ and ϵ_{Nd} of *Piepgras and Wasserburg* [1980, 1982, 1983], *Stordal and Wasserburg* [1986], *Piepgras and Wasserburg* [1987], *Piepgras and Jacobsen* [1988], *Spivack and Wasserburg* [1988], *Bertram and Elderfield* [1993], *Jeandel* [1993], *Henry et al.* [1994], *Shimizu et al.*

Table 1. Comparison of Characteristic Numbers of the CTRL Nd Parametrization of *Rempfer et al.* [2011] and the Parametrization Used in This Study[a]

Experiment	$[Nd]_p/[Nd]_d$ (1)	f_{bs} (g Nd yr^{-1})	I (g Nd)	τ_{Nd} (years)	$J_{[Nd]_d}$ (pmol kg^{-1})	$J_{\epsilon_{Nd}}$ ϵ_{Nd}(1)
CTRL[b]	0.001	5.5· 10^9	4.2· 10^{12}	700	9	1.66
CTRL[c]	0.0014	4.5· 10^9	3.6· 10^{12}	720	11	1.55

[a] $[Nd]_p/[Nd]_d$ is the ratio between particle-associated and dissolved Nd, f_{bs} is the magnitude of the boundary source, I is the global ocean Nd inventory, and τ_{Nd} is the mean residence time of Nd in the ocean (defined as the ratio of I and total sources f_{tot}, i.e., $\tau_{Nd} = I/f_{tot}$). $J_{[Nd]_d}$ and $J_{\epsilon_{Nd}}$ indicate global mean average deviations of simulated from observed $[Nd]_d$ and ϵ_{Nd}, respectively, and are calculated following *Rempfer et al.* [2011, equation 15].
[b] *Rempfer et al.* [2011].
[c] This study.

Table 2. Acronyms for Freshwater Experiments[a]

Experiment	T_{Fw}	Fw	Fw-Region
NA04k005Sv	0.4 kyr	0.05 *Sv*	NA
NA1k005Sv	1 kyr	0.05 *Sv*	NA
NA2k005Sv	2 kyr	0.05 *Sv*	NA
NA20k005Sv	20 kyr	0.05 *Sv*	NA
NA04k030Sv	0.4 kyr	0.3 *Sv*	NA
NA1k030Sv	1 kyr	0.3 *Sv*	NA
NA2k030Sv	2 kyr	0.3 *Sv*	NA
NA20k030Sv	20 kyr	0.3 *Sv*	NA
SO04k005Sv	0.4 kyr	0.05 *Sv*	SO
SO1k005Sv	1 kyr	0.05 *Sv*	SO
SO2k005Sv	2 kyr	0.05 *Sv*	SO
SO20k005Sv	20 kyr	0.05 *Sv*	SO
SO04k030Sv	0.4 kyr	0.3 *Sv*	SO
SO1k030Sv	1 kyr	0.3 *Sv*	SO
SO2k030Sv	2 kyr	0.3 *Sv*	SO
SO20k030Sv	20 kyr	0.3 *Sv*	SO

[a]Freshwater fluxes of different duration (T_{Fw}) and magnitude (Fw) are applied in the North Atlantic (basinwide between 45 and 70°N, NA) and in the Ross and Weddell Sea areas of the model (170–180°W 63–71°S, and 40–60°W 63–71°S, SO). These regions are indicated as light grey areas in Figure 4b.

[1994], *Jeandel et al.* [1998], *Tachikawa et al.* [1999], *Amakawa et al.* [2000], *Lacan and Jeandel* [2001], *Amakawa et al.* [2004], *Vance et al.* [2004], *Tachikawa et al.* [2004], *Lacan and Jeandel* [2004a, 2004b, 2004c, 2005a, 2005b], *Dahlqvist et al.* [2005], *Andersson et al.* [2008], *Amakawa et al.* [2009], *Godfrey et al.* [2009], *Zimmermann et al.* [2009a, 2009b], *Porcelli et al.* [2009], and *Rickli et al.* [2009, 2010]. Further observations of *Elderfield and Greaves* [1982], *Greaves et al.* [1999], and *Carter et al.* [2012] were added to the compilation. As Nd enters the ocean at continental margins at depths shallower than 3000 m, we excluded observations of $[Nd]_d$ and ϵ_{Nd} located in grid cells adjacent to this source from the parameterization procedure. Compared to the study of *Rempfer et al.* [2011] $[Nd]_d$ and ϵ_{Nd} are simulated in reasonable agreement with observations if the parameterization of the reversible scavenging is increased by 40% ($[Nd]_p/[Nd]_d$ = 0.0014) and the magnitude of the boundary source is reduced by ≈18% ($f_{bs} = 4.5 \cdot 10^9$ g Nd yr^{-1}, Figure 3, in the following denoted as CTRL). Further characteristic numbers of the CTRL Nd parameterization of *Rempfer et al.* [2011] and of this study are given in Table 1.

3. Overview of Experiments

[10] In order to examine the effect of changes in MOC, e.g., during idealized sequences of abrupt change on ϵ_{Nd} at the seafloor, we applied periodic varying freshwater fluxes of different amplitude (Fw) and periodicity (T_{Fw}, Table 2) to the North Atlantic (NA experiments) and to the Southern Ocean (SO experiments). In NA experiments perturbations were applied between 45 and 70°N, in SO experiments they were applied to the Ross and Weddell Sea areas of the model (170–180°W, 63–71°S and 40–60°W, 63–71°S respectively, see also Figure 4b). The time pattern of the freshwater-fluxes is triangular in each experiment, i.e. freshwater-fluxes vary linearly between $+Fw$ and $-Fw$ and increase from 0 to $1/4 \cdot T_{Fw}$. Predominantly but not exclusively, positive/negative freshwater-fluxes lead to a weakening/strengthening of the formation of deep-water masses in the corresponding

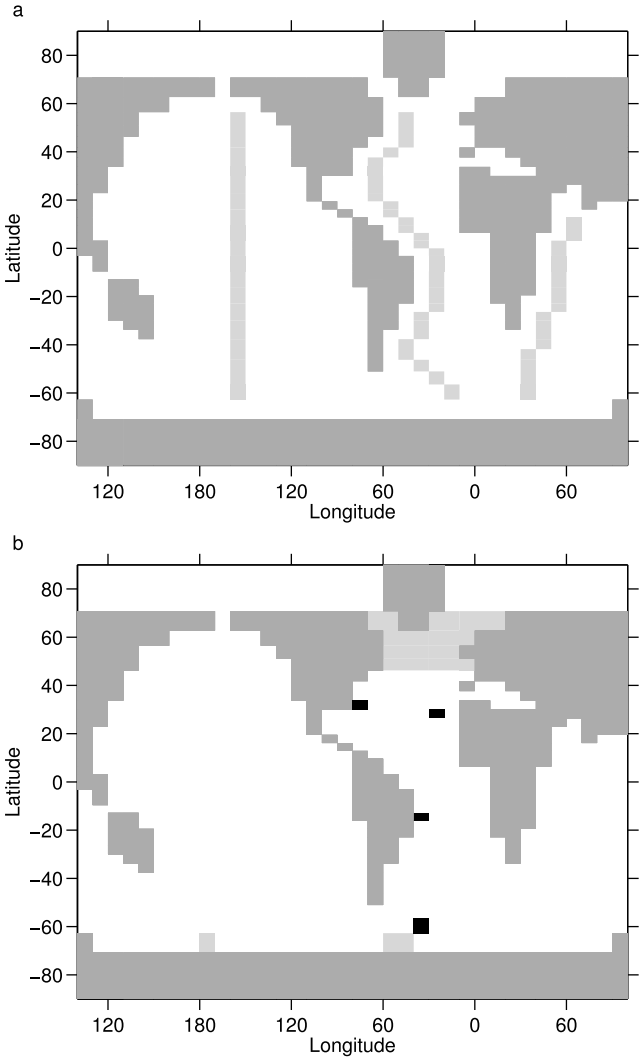

Figure 4. (a) Tracks of Hovmöller plots through the Atlantic, the Indian, and the Pacific oceans as shown in Figures 8 and 11. (b) Black: Sites in the Northwest Atlantic (30–34°N, 70–80°W), the Northeast Atlantic (26–30°N, 20–30°W), the South Atlantic (13–16°S, 30–40°S), and the Southern Ocean (30–40°W, 56–63°S) from which time series are shown in Figures 13 and 14. Light grey: Areas where freshwater-fluxes are applied in the North Atlantic (NA experiments) and in Ross and Weddell Sea areas of the model (SO experiments).

Table 3. Acronyms for Experiments Where Particle Export Fluxes of the CTRL Experiment Were Scaled by Factors 1/2, 1, and 2 in the North Atlantic and the Southern Ocean[a]

Experiment	Scaling Factor	Scaling Region
NATLEXPFL05	0.5	North Atlantic
NATLEXPFL10	1.0	North Atlantic
NATLEXPFL20	2.0	North Atlantic
SOCEXPFL05	0.5	Southern Ocean
SOCEXPFL10	1.0	Southern Ocean
SOCEXPFL20	2.0	Southern Ocean

[a]Freshwater-fluxes (T_{Fw} = 2 kyr; Fw = 0.3 *Sv*) were applied in the North Atlantic and the Ross and Weddell Sea areas of the model, thus corresponding to experiments NA2k030Sv and SO2k030Sv, respectively.

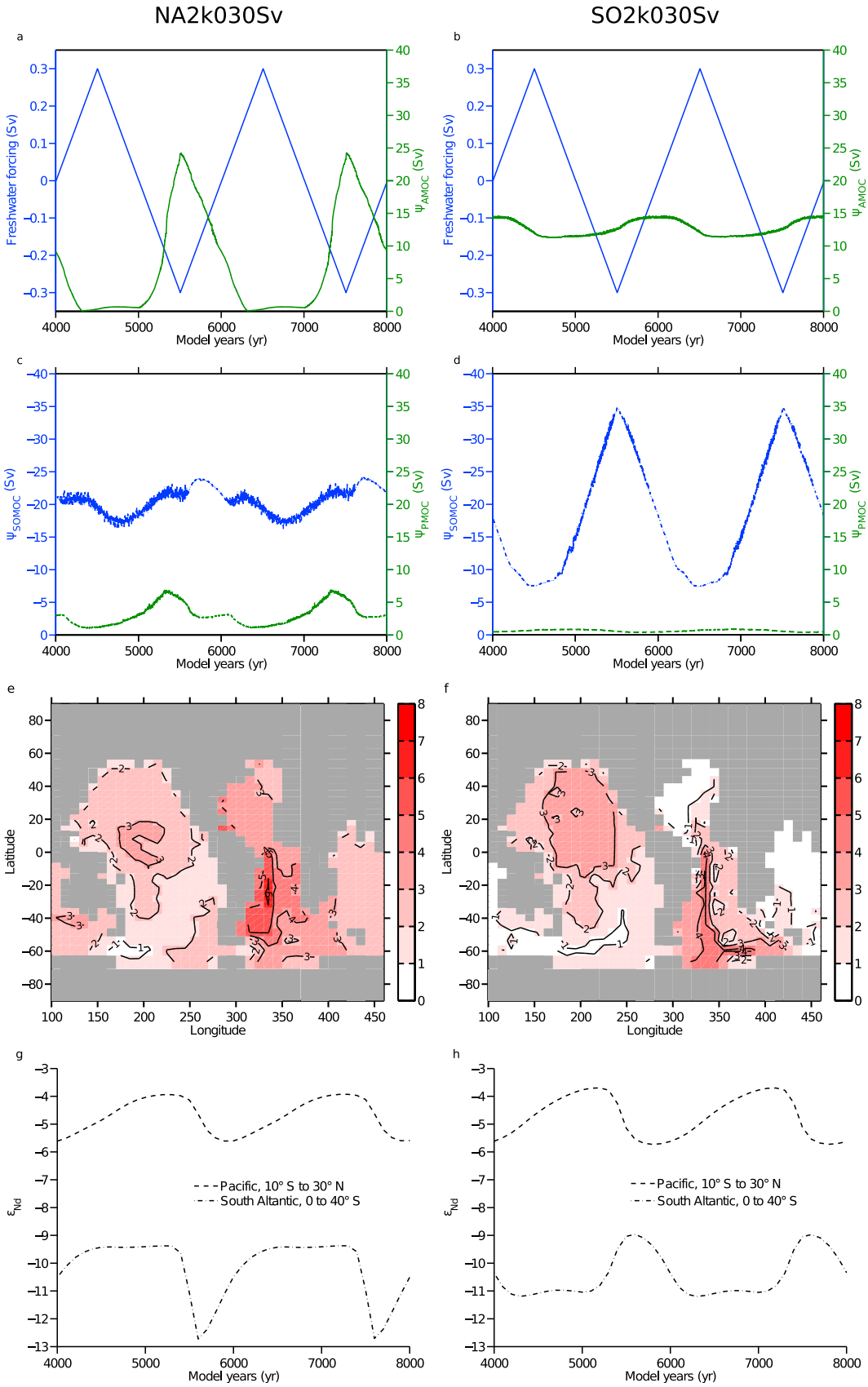
NA2k030Sv
SO2k030Sv
a
b
c
d
e
f
g
h
Freshwater forcing (Sv)
Ψ_{AMOC} (Sv)
Ψ_{SOMOC} (Sv)
Ψ_{PMOC} (Sv)
Model years (yr)
Latitude
Longitude
ϵ_{Nd}
Pacific, 10° S to 30° N
South Altantic, 0 to 40° S

Figure 5

region, i.e., in the formation of NADW and Antarctic Bottom Water (AABW). In general, patterns of changes in experiments where $Fw = 0.1$ and 0.2 *Sv* are intermediate between experiments where $Fw = 0.05$ and 0.3 *Sv*. In NA experiments we decrease the freshwater flux corrections that are applied to match observed atmospheric moisture transport from the Atlantic to the Indo-Pacific from the standard value of 0.34 *Sv* [*Ritz et al.*, 2011b] to 0.17 *Sv*. Reducing this moisture transport allows us to keep variations in maximum AMOC (ψ_{AMOC}) within a reasonable range [*Ganachaud and Wunsch*, 2000; *Talley et al.*, 2003]. Leaving the moisture transport unchanged would require a larger amount of freshwater for a shut down of the formation of NADW and would lead to stronger AMOC during on-states.

[11] In addition to a general evaluation of how well ϵ_{Nd} reflects changes in overturning strength, the wide range in the formation of NADW and AABW, resulting from our freshwater experiments, allows us to examine whether ϵ_{Nd} can be used to differentiate between a weakening and a cessation of the formation of NADW and AABW, respectively. Moreover, the application of freshwater-fluxes either to the North Atlantic or the Southern Ocean, largely affects the formation of one single water mass only. This makes it possible to evaluate whether inferences on the origin of changes in ocean circulation can be derived from the corresponding large-scale pattern of ϵ_{Nd} at the seafloor.

[12] In our model export fluxes of biogenic particles opal, $CaCO_3$, and POC are calculated from prognostic equations and therefore vary, e.g., with changes in ocean circulation. The magnitude of particle export fluxes affects the magnitude of the sink of Nd and thus its mean residence time (τ_{Nd}), which in turn affects the water mass property of ϵ_{Nd} [*Rempfer et al.*, 2011]. To evaluate the effect of changes in the magnitude of export fluxes on ϵ_{Nd}, we perform additional experiments where we scale particle fields of opal, $CaCO_3$, and POC from the CTRL by factors 0.5, 1 and 2 (see Table 3 for a description of experiments).

[13] As ϵ_{Nd} in sediment records has been reported to reflect ϵ_{Nd} in bottom water [e.g., *Piepgras and Wasserburg*, 1980; *Frank*, 2002] we present results of ϵ_{Nd} from lowermost grid cells. In our approach Nd enters the ocean across the sediment-water interface between the sea surface and 3000 m depth [*Rempfer et al.*, 2011] and we therefore focus on results from depths greater than 3000 m.

4. Freshwater Experiments: Variations in MOC Strength and ϵ_{Nd}

[14] Meridional Overturning Circulation below the wind driven mixed layer is represented by a stream function which can take positive and negative values (Figures 1a–1o). A positive (negative) stream function is referred to as a clockwise (counterclockwise) overturning circulation.

[15] In the modern steady state (CTRL) a clockwise overturning cell in the North Atlantic, with a strength of about 14 *Sv*, is associated with the formation of NADW. About 1 *Sv* of AABW is advected northward below the tongue of NADW via counterclockwise overturning in the deep South Atlantic (Figure 1a). A southern and a northern cell can also be distinguished in the Pacific. However, in contrast to the North Atlantic, almost no deep convection takes place in the North Pacific and large parts of the basin are filled with southern source water (i.e., AABW, Figure 1b). AABW is formed in the Southern Ocean and is then advected northward into the different basins (Figure 1c).

[16] On and off-states for experiments NA2k030Sv and SO2k030Sv are shown in Figures 1d–1o as representative examples.

[17] During NA2k030Sv on-state clockwise overturning in the Atlantic is stronger than in the CTRL (22 instead of 13 *Sv*) and the Atlantic basin is largely filled by NADW. Accordingly, no AABW is advected northward from the Southern Ocean (Figure 1d).

[18] Compared to the Atlantic, changes are less pronounced in the Pacific Ocean. Northward advection of southern source water, associated with counterclockwise circulation in the deep Pacific, is stronger by about 1 *Sv* and some intermediate water is formed in the North Pacific (Figure 1e).

[19] Overturning in the deep Southern Ocean is hardly affected by the changes in the North Atlantic (Figure 1f).

[20] During NA2k030Sv off-state overturning is sluggish in the Atlantic basin. No NADW is formed in the North Atlantic and hence no northern source water is advected southward (Figures 1g and 1i). Instead, southern source water fills large parts of the basin (Figure 1g).

[21] Compared to the Atlantic Ocean and similar in magnitude to the on-state, changes are less pronounced in the Pacific, where northward advection of southern source water is weaker than in the CTRL by about 1 *Sv* (Figure 1h).

[22] During SO2k030Sv on-state clockwise overturning in the North Atlantic is slightly weaker than in the CTRL (11 *Sv* instead of 13 *Sv*, Figure 1j). At the same time, overturning is considerably stronger in the Southern Ocean (Figure 1l) from where about 7 *Sv* of southern source water are advected northward in the Atlantic basin. Due to the increase in the formation of AABW, a larger fraction of the Atlantic basin is filled by this water mass, and NADW is confined to shallower depths (Figure 1j).

[23] The increased formation of AABW can also be observed in the Pacific Ocean, where compared to the CTRL, advection of southern source water to the north is increased by about 6 *Sv* (Figure 1k).

[24] During SO2k030Sv off-state the formation of AABW almost ceases (Figure 1o) and no southern source water is advected northward in the Atlantic (Figure 1m). Clockwise

Figure 5. Exemplary results from experiments (left) NA2k030Sv and (right) SO2k030Sv (see Table 2 for further details). (a, b) Freshwater fluxes (blue) and resulting changes in ψ_{AMOC} (green), (c, d) ψ_{PMOC} (green) and ψ_{SOMOC} (blue). Note that the direction of y-axes that indicate ψ_{SOMOC} is reverse. Areas where freshwater-fluxes are applied are indicated in light grey in Figure 4b. (e, f) Global map of absolute differences between maximum and minimum ϵ_{Nd} ($\Delta\epsilon_{Nd}$). (g, h) Spatially averaged time series from the North Pacific and the Southern Ocean indicating the effect of changes in ψ_{AMOC} and ψ_{SOMOC} on ϵ_{Nd} in the corresponding region (see details on panels).

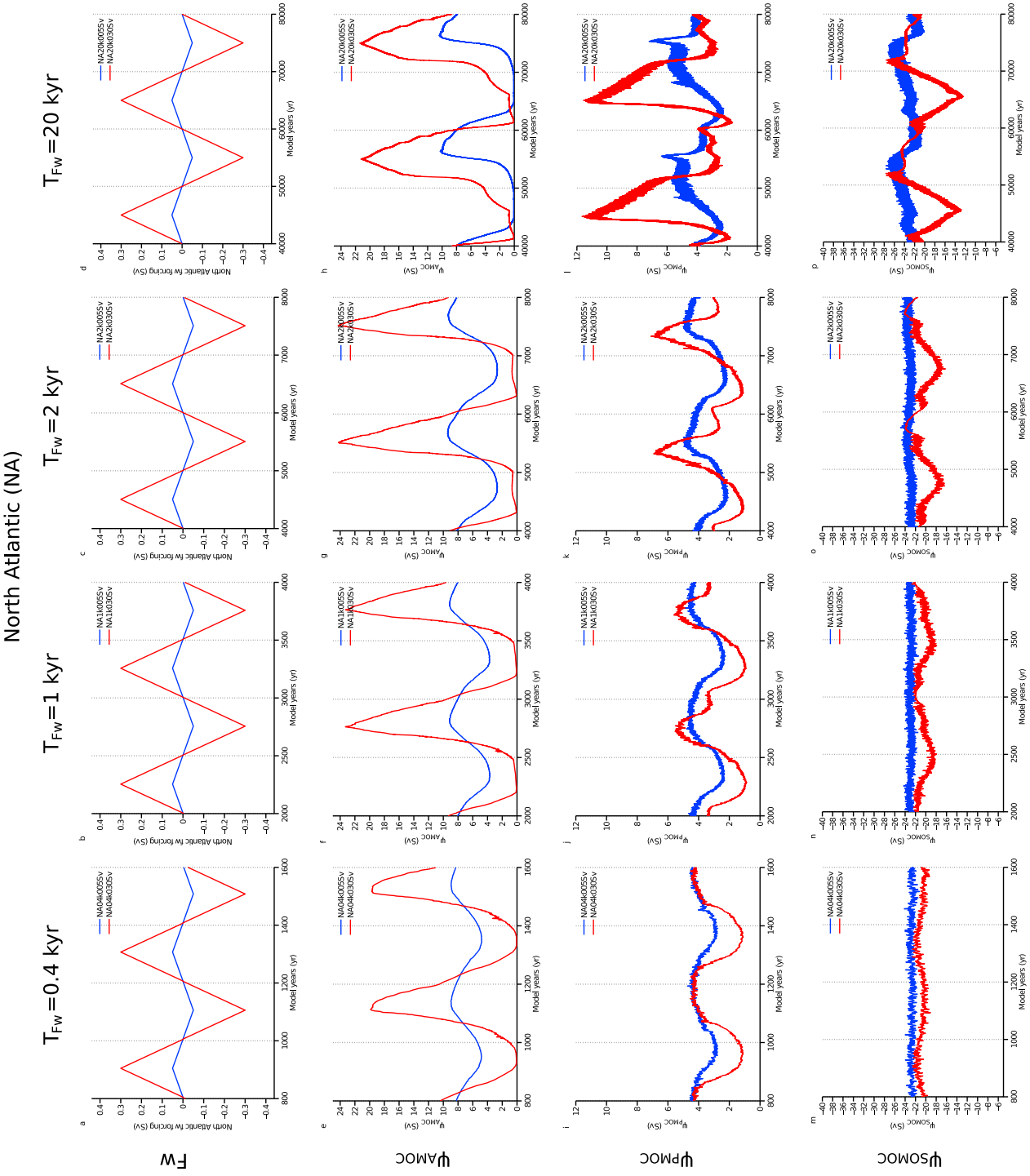
North Atlantic (NA)
T_Fw=0.4 kyr
T_Fw=1 kyr
T_Fw=2 kyr
T_Fw=20 kyr
FW
ΨAMOC
ΨPMOC
ΨSOMOC
North Atlantic fw forcing (Sv)
Model years (yr)
NA04k005Sv
NA04k030Sv
NA1k005Sv
NA1k030Sv
NA2k005Sv
NA2k030Sv
NA20k005Sv
NA20k030Sv

Figure 6

overturning in the North Atlantic is only slightly weaker than in the CTRL (11 *Sv* instead of 13 *Sv*) and as a result the basin is largely filled by northern source water (Figure 1j). Advection of southern source water to the north is also reduced in the Pacific Ocean (by about 2 *Sv* compared to the CTRL, Figure 1k).

[25] In the following, results of ϵ_{Nd} are presented in Hovmöller plots along tracks through the Atlantic, the Indian, and the Pacific oceans. The corresponding tracks are indicated in Figure 4a. Moreover, time series of ϵ_{Nd} are shown from selected sites in the Northwest Atlantic, the Northeast Atlantic, the South Atlantic and the Southern Ocean. Their locations are indicated in Figure 4b. Areas where freshwater-fluxes are applied in the NA and SO experiments are also indicated in Figure 4b.

[26] Before showing results from a number of experiments, and in order to better illustrate the effects of changes in overturning on ϵ_{Nd}, we will explain two of the experiments, one of each NA and SO experiments, in greater detail (Figure 5). Applying periodically varying freshwater-pulses to the North Atlantic and the Ross and Weddell Sea areas of the model affects maximum AMOC (ψ_{AMOC}), maximum PMOC (ψ_{PMOC}) and the minimum global MOC (ψ_{SOMOC}) to some extent (Figures 5a–5d). However, while in experiment NA2k030Sv major changes are confined to ψ_{AMOC}, changes are largest in ψ_{SOMOC} in experiment SO2k030Sv. Overall, ψ_{AMOC} and ψ_{SOMOC} are roughly in phase with freshwater-perturbations. Both become weaker when freshwater is added and stronger when freshwater is removed from the corresponding region in the North Atlantic and the Southern Ocean (Figures 5a and 5c and 5b and 5d).

[27] Global maps of maximum variations in ϵ_{Nd} ($\Delta\epsilon_{Nd}$, i.e., the maximum variation in ϵ_{Nd}; $\epsilon_{Nd\max} - \epsilon_{Nd\min}$) indicate that ϵ_{Nd} is affected throughout the global ocean and that variations in $\Delta\epsilon_{Nd}$ are not globally uniform (Figures 5g and 5f). In experiment NA2k030Sv $\Delta\epsilon_{Nd}$ is particularly large in the South Atlantic where main water masses alternate during on and off-states as well as along the western boundary in the North Atlantic where NADW is advected southward during on-states. Similarly, in experiment SO2k030Sv $\Delta\epsilon_{Nd}$ is large in the South Atlantic. However, $\Delta\epsilon_{Nd}$ is of similar magnitude in the Southern Ocean in the area where formation of AABW takes place and is smaller in the North Atlantic where changes in addition are largely confined to the eastern boundary.

[28] Spatially averaged time series from North Pacific and South Atlantic regions (10 to 50°N and from the equator to 40°S, respectively) show that ϵ_{Nd} increases to more positive values due to a shutdown of the formation of NADW and drops to more negative values following a resumption of the formation of NADW (Figure 5g). On the other hand, the temporal evolution of ϵ_{Nd} in the North Pacific and the South Atlantic is in antiphase in experiment SO2k030Sv (Figure 5h). In this case, ϵ_{Nd} becomes more negative in the South Atlantic and more positive in the central Pacific due to a reduction in ψ_{SOMOC}. Correspondingly, ϵ_{Nd} increases to more positive values in the South Atlantic and decreases to more negative values in the central Pacific following an increase in ψ_{SOMOC}.

[29] Overall, global maps of $\Delta\epsilon_{Nd}$ and spatially averaged time series of ϵ_{Nd} indicate substantial differences between NA and SO experiments.

4.1. Northern Perturbation

[30] Adding freshwater to the North Atlantic (NA experiments) leads to a reduction in ψ_{AMOC}, while removing freshwater leads to an increase (Figures 6e–6h). In NA experiments ψ_{AMOC} varies between about 5 and 9 *Sv* (for T_{Fw} = 0.4 kyr and Fw = 0.05 *Sv*), and between about 0 and 24 *Sv* (for T_{Fw} = 2 kyr and Fw = 0.3 *Sv*). ψ_{PMOC}, varies between about 3 and 5 *Sv* (for T_{Fw} = 0.4 kyr and Fw = 0.05 *Sv*), and between about 2 and 12 *Sv* (for T_{Fw} = 20 kyr and Fw = 0.3 *Sv*). Variations in ψ_{PMOC} are in phase with variations in ψ_{AMOC} for T_{Fw} = 0.4, 1, 2 kyr, but are in antiphase for T_{Fw} = 20 kyr (Figures 6i–6l). ψ_{SOMOC} varies between about –22 and –24 *Sv* (for T_{Fw} = 0.4 kyr and Fw = 0.05 *Sv*) and between about –12 and –28 *Sv* (for T_{Fw} = 20 kyr and Fw = 0.3 *Sv*, Figures 6m–6p). While smallest variations in general are associated with T_{Fw} = 0.4 kyr and Fw = 0.05 *Sv*, largest variations are not necessarily associated with experiments where T_{Fw} = 20 kyr, but rather with experiments where T_{Fw} = 2 kyr. This is probably due to long-term basin-scale adjustments in the former case.

[31] In general, ϵ_{Nd} is affected only to a small extent in experiments where both Fw and T_{Fw} are small. On the other hand, ϵ_{Nd} varies considerably if T_{Fw} and/or Fw are larger (Figure 7). Apart from T_{Fw} and Fw the magnitude of $\Delta\epsilon_{Nd}$ also depends on the geographic location.

[32] In the deep Atlantic, $\Delta\epsilon_{Nd}$ is largest (up to 5 ϵ_{Nd}-units) between the equator and 40°S, where northern and southern source waters alternate during AMOC-on and AMOC-off-states.

[33] Regarding the deep Pacific, $\Delta\epsilon_{Nd}$ is largest (up to 4ϵ_{Nd}-units) in the central North Pacific. Note that $\Delta\epsilon_{Nd}$ in the Indian exceeds 2 ϵ_{Nd}-units only in a few, particularly NA experiments (Figures 7d, 7g, 7h, and 10h), and only slightly exceeds 1 ϵ_{Nd}-units in the other experiments.

[34] Overall, in the Atlantic, the Indian and the Pacific relatively negative ϵ_{Nd} during AMOC on-states is replaced by more positive ϵ_{Nd} during AMOC off-states (Figures 8e–8p). While northern source water is exported from the North Atlantic in periods of strong AMOC, less or no northern source water is advected southward in case of a sluggish or ceased AMOC. Instead, a larger part of the Atlantic is filled by southern source water leading to more positive ϵ_{Nd} (Figures 8e–8h). Accordingly, less relatively negative ϵ_{Nd} is advected from the Atlantic to the Indian and the Pacific, in periods of a sluggish or ceased AMOC, and thus ϵ_{Nd} increases in these basins as well (Figures 8i–8p).

Figure 6. (a–d) Freshwater fluxes of different periods (from left to right, T_{Fw} = 0.4, 1, 2, 20 kyr) and amplitudes (Fw = 0.05, 0.3 *Sv*) that are applied to the North Atlantic in NA experiments, as well as (e–h) resulting strength of AMOC (ψ_{AMOC}), (i–l) PMOC (ψ_{PMOC}), and (m–p) SOMOC (ψ_{SOMOC}) in *Sv* (10^6 m^3 s^{-1}). Note that the direction of y-axes that indicate ψ_{SOMOC} is reverse. The area where freshwater-fluxes are applied is indicated in light grey in Figure 4b.

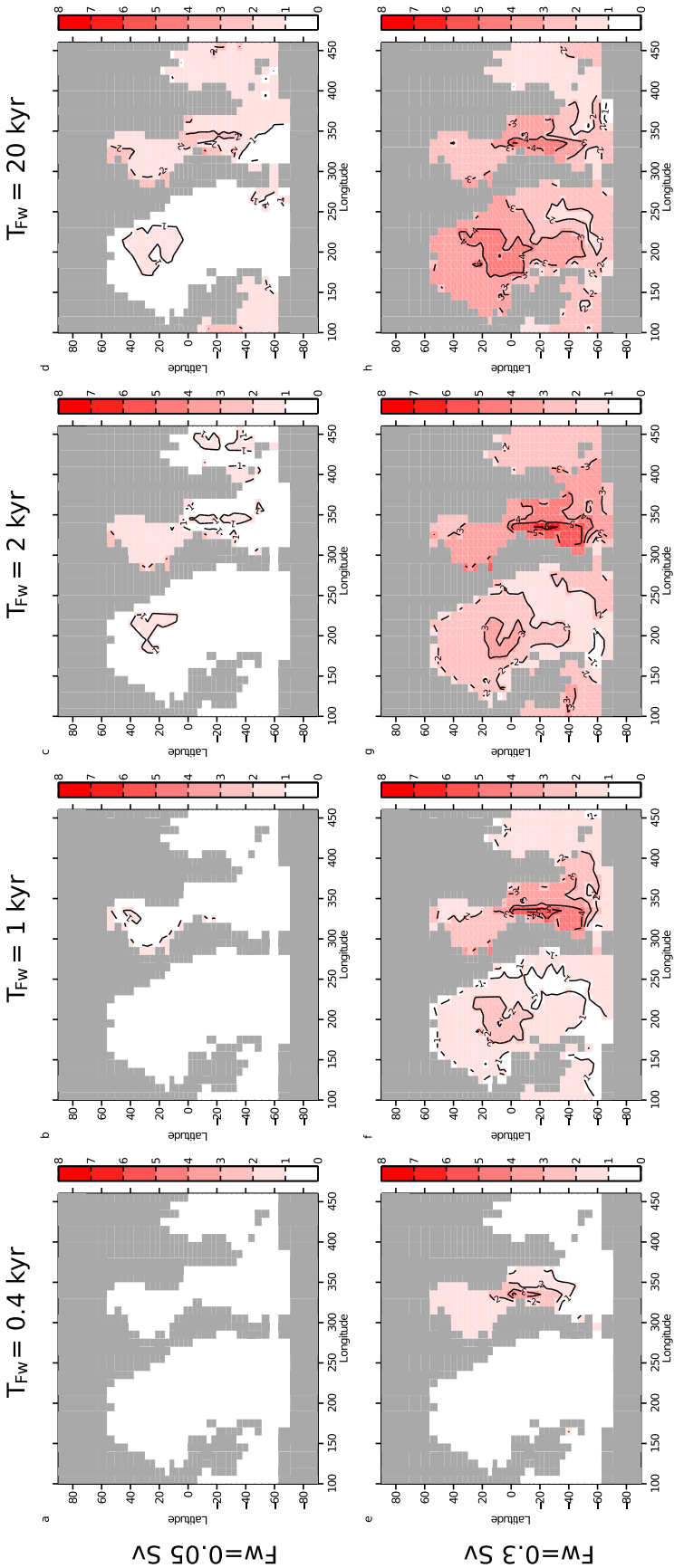

Figure 7. Global maps of $\Delta\epsilon_{Nd}$, corresponding to the absolute difference between maximum and minimum ϵ_{Nd}, at the seafloor. Results are from experiments where one single positive and negative freshwater-pulse of periods T_{Fw} = (a, e) 0.4, (b, f) 1, (c, g) 2, and (d, h) 20 kyr and amplitudes $Fw = 0.05$ and 0.3 *Sv* (Figures 7a–7d and 7e–7h, respectively) was applied to the North Atlantic (indicated as light grey areas in Figure 4b).

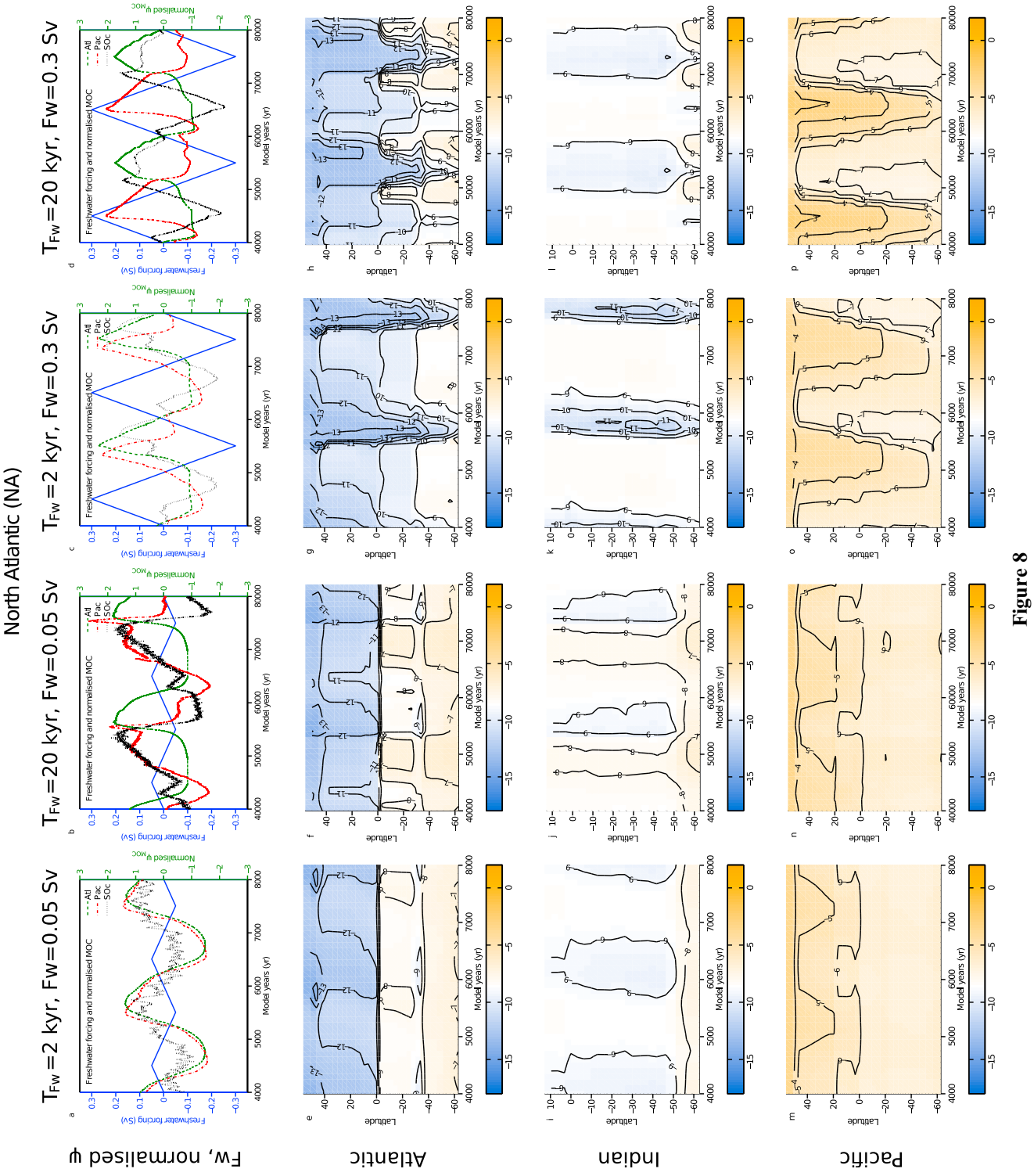
North Atlantic (NA)
T_{Fw}=2 kyr, Fw=0.05 Sv
T_{Fw}=20 kyr, Fw=0.05 Sv
T_{Fw}=2 kyr, Fw=0.3 Sv
T_{Fw}=20 kyr, Fw=0.3 Sv
Fw, normalised ψ
Atlantic
Indian
Pacific
Freshwater forcing and normalised MOC
Atl
Pac
SOc
Freshwater forcing (Sv)
Normalised ψMOC
Model years (yr)
Latitude

Figure 8

[35] In experiment NA20k030Sv effects on ϵ_{Nd} in the Pacific are larger than in other experiments (Figures 7h and 8p). In this experiment PMOC is quite strong during AMOC off-states (up to 12 *Sv*, Figure 6l) and an overturning cell emerges in the North Pacific leading to the formation of intermediate water (not shown). This probably increases the export of relatively positive ϵ_{Nd} out of the Pacific basin leading to less negative ϵ_{Nd} in the Indian as well as in the Atlantic during AMOC on-states.

[36] In general, effects of variations in overturning strength on ϵ_{Nd} are almost identical during the first period and in following periods of freshwater forcing.

4.2. Southern Perturbation

[37] The effect of adding and removing freshwater to and from the Ross and Weddell Sea areas of the model ("Southern Perturbation", SO experiments, Figure 9), differs from NA experiments. For example, while major changes occur in ψ_{SOMOC}, ψ_{AMOC} is only slightly affected in most of the experiments (Figures 9e–9h). An exception is experiment SO20k030Sv in which ψ_{AMOC} varies strongly (between about 2 and 15 *Sv*). Variations in ψ_{PMOC} are relatively small, even in experiment SO20k030Sv (between 1 and 4 *Sv*, Figures 9i–9l). In contrast, variations in ψ_{SOMOC} are considerable even in experiments where T_{Fw} and Fw are small (between –15 and –20 *Sv* for T_{Fw} = 0.4 kyr and Fw = 0.05 *Sv*, Figures 9m–9p). Not surprisingly, largest variations are observed for T_{Fw} = 20 kyr and Fw = 0.3 *Sv* (between –8 and –38 *Sv*). In general, ψ_{SOMOC} decreases/increases in phase with the application of positive/negative freshwater-fluxes to the Ross and Weddell Sea areas of the model (in contrast to ψ_{AMOC} and ψ_{PMOC}, which both are only roughly in phase with freshwater-fluxes).

[38] Similar to the NA experiments, ϵ_{Nd} varies with changes in overturning strength and $\Delta\epsilon_{Nd}$ also depends on the geographic location. However, the spatial pattern of $\Delta\epsilon_{Nd}$ in SO experiments is different (Figure 10). Major variations in ϵ_{Nd} are confined to the Atlantic section of the Southern Ocean (up to 4 ϵ_{Nd}-units) and the North Pacific (up to 3 ϵ_{Nd}-units). $\Delta\epsilon_{Nd}$ is generally small in the Indian (up to 1 ϵ_{Nd}-unit). The effect on ϵ_{Nd} in the Atlantic reaches further north for larger amplitudes of T_{Fw} or/and Fw. In addition, $\Delta\epsilon_{Nd}$ in the North Atlantic and in the North Pacific increases with increasing amplitude of T_{Fw} or/and Fw. An important feature is that effects on ϵ_{Nd} in the North Atlantic are confined to the eastern part of the basin and that smaller effects on ϵ_{Nd} arise in the western part of the North Atlantic (Figures 10e–10g), except for experiment SO20k030Sv (Figure 9h). Therefore, our results indicate differences between NA and SO experiments.

[39] As mentioned above, effects on ϵ_{Nd} are different in experiment SO20k030Sv (Figure 10h). In this experiment AMOC is relatively weak (down to 2 *Sv*, Figure 9h). Therefore, southward transport of NADW-like ϵ_{Nd} is reduced leading to more southern source water-like ϵ_{Nd} in the entire North Atlantic, not only in the eastern part of the basin.

[40] Another important difference between NA and SO experiments is that changes in ϵ_{Nd} are not of equal sign in the Atlantic, the Indian and the Pacific in SO experiments: In the Atlantic ϵ_{Nd} is slightly more negative during periods of weak SOMOC and considerably more positive during periods of strong SOMOC (Figures 11e–11h). A similar pattern, although only weakly pronounced, emerges in the Indian (Figure 11i–11l). However, in the Pacific the pattern is vice versa, i.e., ϵ_{Nd} is considerably more positive during periods of weak SOMOC and slightly more negative during periods of strong SOMOC (Figures 11m–11p). In most of the SO experiments ψ_{AMOC} and ψ_{PMOC} are affected only slightly, and only ψ_{SOMOC} varies over a large range (Figure 9). Changes in ϵ_{Nd} are therefore mainly due to changes in ψ_{SOMOC}. ϵ_{Nd} of AABW is intermediate compared to ϵ_{Nd} in the North Atlantic and the North Pacific. Thus, if ψ_{SOMOC} is strong, export of relatively positive AABW-like ϵ_{Nd} from the Southern Ocean into the Atlantic is more pronounced, leading to a shift to more positive ϵ_{Nd} in this basin. At the same time, export of relatively negative AABW-like ϵ_{Nd} from the Southern Ocean into the Pacific is enhanced, leading to a shift to more negative ϵ_{Nd}. On the other hand, ϵ_{Nd} is more NADW-like in the Atlantic and more North Pacific-like in the Pacific in case of weak ψ_{SOMOC}. As ϵ_{Nd} in the Indian is generally AABW-like, effects are small in this basin.

[41] In contrast, in NA experiments mainly the formation of NADW is affected which carries the most negative ϵ_{Nd}. An increase/decrease in strength of ψ_{AMOC} thus leads to more negative/positive ϵ_{Nd} in the Atlantic, the Indian and the Pacific.

4.3. A Note on End-Member Stability

[42] The stability of the corresponding end-member is of importance for the interpretation of downstream variations in ϵ_{Nd} as changes in overturning circulation [e.g., *Piotrowski et al.*, 2004]. Figure 12 illustrates Atlantic and Pacific cross-sections of differences in ϵ_{Nd} at times when most positive and most negative ϵ_{Nd} occur in experiments NA2k030Sv and SO2k030Sv (see the figure caption for more details). It becomes clear, that changes in ϵ_{Nd} at sites of deep-water formation in the North Atlantic or the Southern Ocean end-member are smaller than further downstream (by about 3–4 ϵ_{Nd}-units). Besides, in case of experiment NA2k030Sv, the small changes in the North Atlantic end-member are not

Figure 8. (a–d) Freshwater forcing (*Sv*) and resulting normalized changes in ψ_{AMOC}, ψ_{PMOC}, and ψ_{SOMOC}. In case of ψ_{SOMOC} absolute values have been calculated before normalization. Hovmöller plots indicating the temporal evolution of ϵ_{Nd} along the western boundary of (e–h) the Atlantic and (i–l) the Indian as well as through (m–p) the central Pacific. Courses of Atlantic, Indian and Pacific tracks are indicated in Figure 4a. Results are from experiments where freshwater fluxes of different amplitudes (Fw = 0.05 *Sv* (first and third columns) and Fw = 0.3 *Sv* (second and fourth columns)) and periods (T_{Fw} = 2 kyr (first and third columns) and T_{Fw} = 20 kyr (second and fourth columns)) are applied to the North Atlantic. The area where freshwater-fluxes are applied is indicated in light grey in Figure 4b.

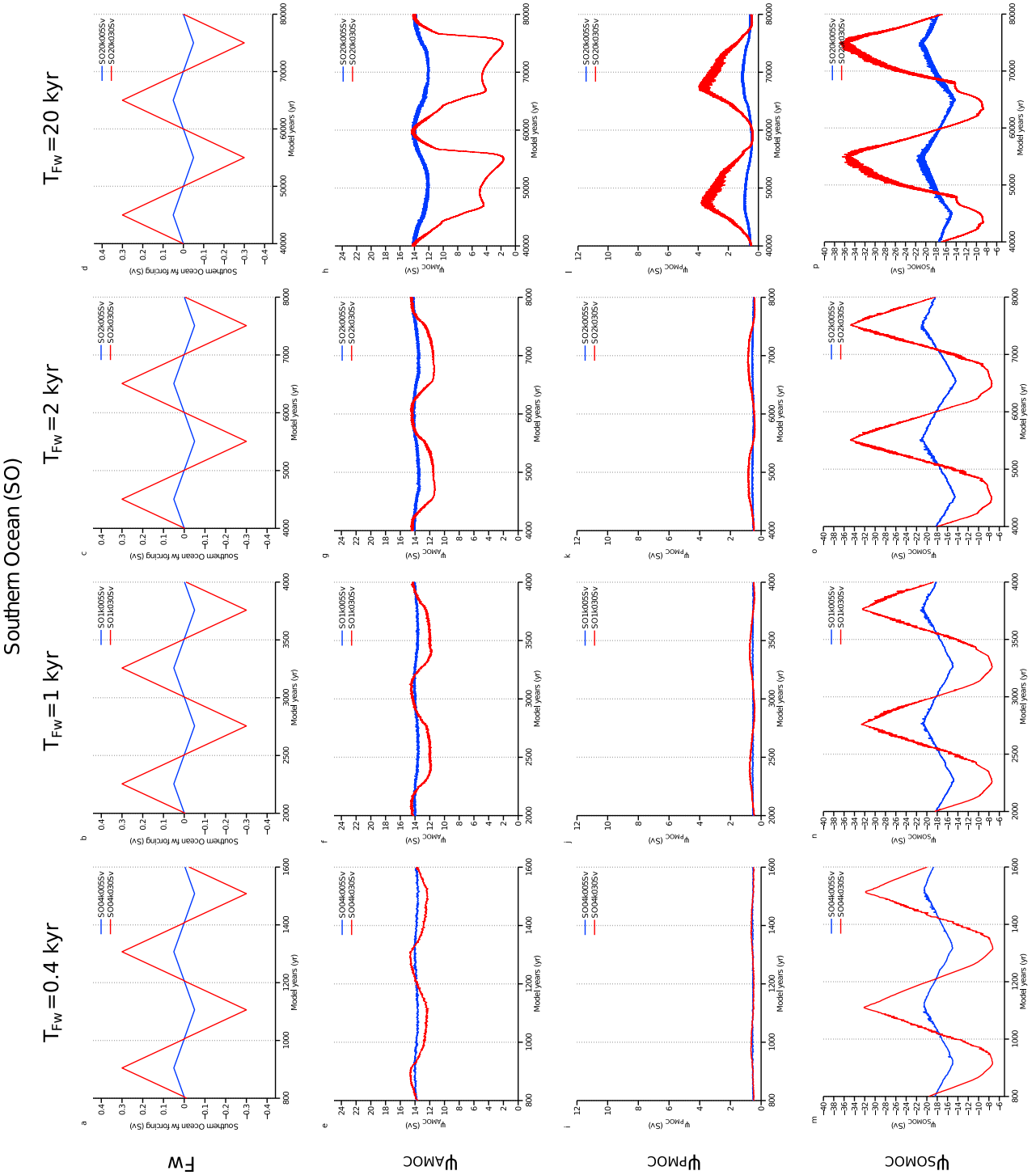
Southern Ocean (SO)
T_Fw=0.4 kyr
T_Fw=1 kyr
T_Fw=2 kyr
T_Fw=20 kyr
FW
ΨAMOC
ΨPMOC
ΨSOMOC
Southern Ocean fw forcing (Sv)
Model years (yr)
SO04k005Sv
SO04k030Sv
SO10k005Sv
SO10k030Sv
SO20k005Sv
SO20k030Sv

Figure 9

uniform in sign. Taken together, this indicates that in our modeling experiments where overturning strength varies on millennial-scale, the observed changes in ϵ_{Nd} are largely due to changes in water mass distribution and that effects of changes in end-member composition are relatively small.

5. Effect of Changes in Particle Export Fluxes on ϵ_{Nd}

[43] Nd is adsorbed onto particle surfaces and, as particles are subject to gravitational force, is transported to depth and finally buried in sediments if particles reach the seafloor [*Bertram and Elderfield*, 1993; *Goldstein and Hemming*, 2003; *Siddall et al.*, 2008; *Arsouze et al.*, 2009; *Rempfer et al.*, 2011]. Any change in particle export fluxes therefore affects the efficiency of the sink of Nd and consequently its mean residence time in the ocean [*Rempfer et al.*, 2011]. It was reported that reorganizations in ocean circulation affect the marine ecosystem in the Atlantic as well as in the global ocean [*Marchal et al.*, 1998; *Schmittner*, 2005; *Yasuhara et al.*, 2008; *Tschumi et al.*, 2008]. Export fluxes of opal, calcite and POC were also affected throughout the global ocean in our experiments (not shown). In addition, it was reported that changes in particle export fluxes introduce additional complication in the interpretation of paleoceanographic tracers in terms of changes in meridional overturning (such as Pa/Th) [e.g., *Siddall et al.*, 2007; *Keigwin and Boyle*, 2008; *Lippold et al.*, 2009]. Although, in contrast to Pa and Th, ^{143}Nd and ^{144}Nd are not known to be subject to preferential scavenging by certain particle types, changes in the magnitude of particle fluxes have the potential to affect the water mass property of ϵ_{Nd} [*Rempfer et al.*, 2011].

[44] In experiments of *Schmittner* [2005], in which AMOC was shut down due to the application of a freshwater-flux, effects on marine ecosystems were not confined to but were largest in the North Atlantic, i.e., in the region where shoaling of the mixed layer prevents upwelling of nutrients. Independent of the exact global pattern and magnitude of changes in nutrient supply and thus export fluxes, we examine the overall effect of variations in export production on ϵ_{Nd} by comparing simulated ϵ_{Nd} from freshwater experiments (NA2k030Sv and SO2k030Sv) where we keep particle fluxes constant at different levels. Therefore, we scale particle export fluxes of CTRL (Figure 2) by factors 1/2, 1, and 2, in the North Atlantic (light grey area in Figure 4b) and in the entire Southern Ocean (south of 34°S), respectively (see Table 3 for a description of experiments). Figure 13 illustrates time series of ϵ_{Nd} at four different sites (Northwest Atlantic, North East Atlantic, South Atlantic, Southern Ocean, locations are indicated in Figure 4b) resulting from these experiments. As changes in ocean overturning circulation are the same as in experiments NA2k030Sv and SO2k030Sv, differences in ϵ_{Nd} can be attributed to changes in particle export fluxes.

[45] Although at each site absolute values of ϵ_{Nd} are affected to some extent, overall patterns in ϵ_{Nd} do not differ much between individual experiments. However, note that $\Delta\epsilon_{Nd}$ is more pronounced in experiments where export fluxes are scaled by a factor of 2 (red), compared to experiments where a factor of 1/2 (blue) is applied. These differences as well as differences in absolute values of ϵ_{Nd} are due to the effect of an increase/decrease in the efficiency of the sink on τ_{Nd}. τ_{Nd} decreases/increases in the corresponding case and results in a more/less pronounced inter-basin gradient. Besides scaling export fluxes of all particle types in tandem, we evaluated the effect of scaling export fluxes of POC, opal and calcite individually. Not surprisingly, effects on ϵ_{Nd} are largest if scaling is applied to POC, opal and calcite simultaneously. Results from these experiments are not shown, but lay within the colored areas (Figure 13).

6. Further Inferences From $\Delta\epsilon_{Nd}$

6.1. Slowdown Versus Shutdown of Ocean Overturning

[46] For the interpretation of ϵ_{Nd} in terms of past circulation changes it is of interest whether the magnitude of changes in overturning can be inferred from variations in ϵ_{Nd}. As we have shown in Figures 7 and 10 as well as in Figures 8 and 11, different magnitudes and durations of changes in overturning circulation lead to different magnitudes of $\Delta\epsilon_{Nd}$ in the global ocean. This suggests that information about changes in the rate of the MOC can be obtained from changes in ϵ_{Nd}. To further examine this suggestion, scatterplots of ϵ_{Nd} versus ψ_{AMOC} and ψ_{SOMOC} at four different sites in the Atlantic are shown in Figure 14.

[47] In NA experiments ϵ_{Nd} in the Atlantic is rather positive for weaker AMOC and rather negative for stronger AMOC (Figures 14a, 14e, 14i, and 14m). ψ_{SOMOC} varies only little in NA experiments, except for experiment NA20k030Sv, and the relationship between ϵ_{Nd} and ψ_{SOMOC} is therefore generally less pronounced (Figures 14b, 14f, 14j, and 14n). Overall, the relationship between ϵ_{Nd} and ψ_{AMOC} or ψ_{SOMOC} is not unequivocal at any of the sites as the range of ϵ_{Nd} is large for given values of ψ_{AMOC} and ψ_{SOMOC}. For a quantitative reconstruction of ψ_{AMOC} or ψ_{SOMOC} based on a given value of ϵ_{Nd} the points in the scatter plots needed to lay on a straight line. From our experiments it therefore appears that it is not possible to assign a unique strength of ψ_{AMOC} or ψ_{SOMOC} to a given value of ϵ_{Nd}.

[48] Similar to ψ_{SOMOC} in NA experiments, ψ_{AMOC} varies only little in SO experiments (except for experiment SO20k030Sv). Therefore, no close relationship can be detected between ϵ_{Nd} and ψ_{AMOC}, except for experiment SO20k030Sv (Figures 14c, 14g, 14k, and 14o). On the other hand, distinct almost linear relationships exist between ϵ_{Nd}

Figure 9. Freshwater fluxes of different periods (from left to right, T_{Fw} = 0.4, 1, 2, 20 kyr) and amplitudes (Fw = 0.05 *Sv* (first and third columns) and Fw = 0.3 *Sv* (second and fourth columns)) that are applied to the Ross and Weddell Sea areas of the model in (a–d) NA experiments, as well as resulting strength of (e–h) AMOC (ψ_{AMOC}), (i–l) PMOC (ψ_{PMOC}), and (m–p) SOMOC (ψ_{SOMOC}) in *Sv* (10^6 m^3 s^{-1}). Note that the direction of y-axes that indicate ψ_{SOMOC} is reverse. The area where freshwater-fluxes are applied is indicated in light grey in Figure 4b.

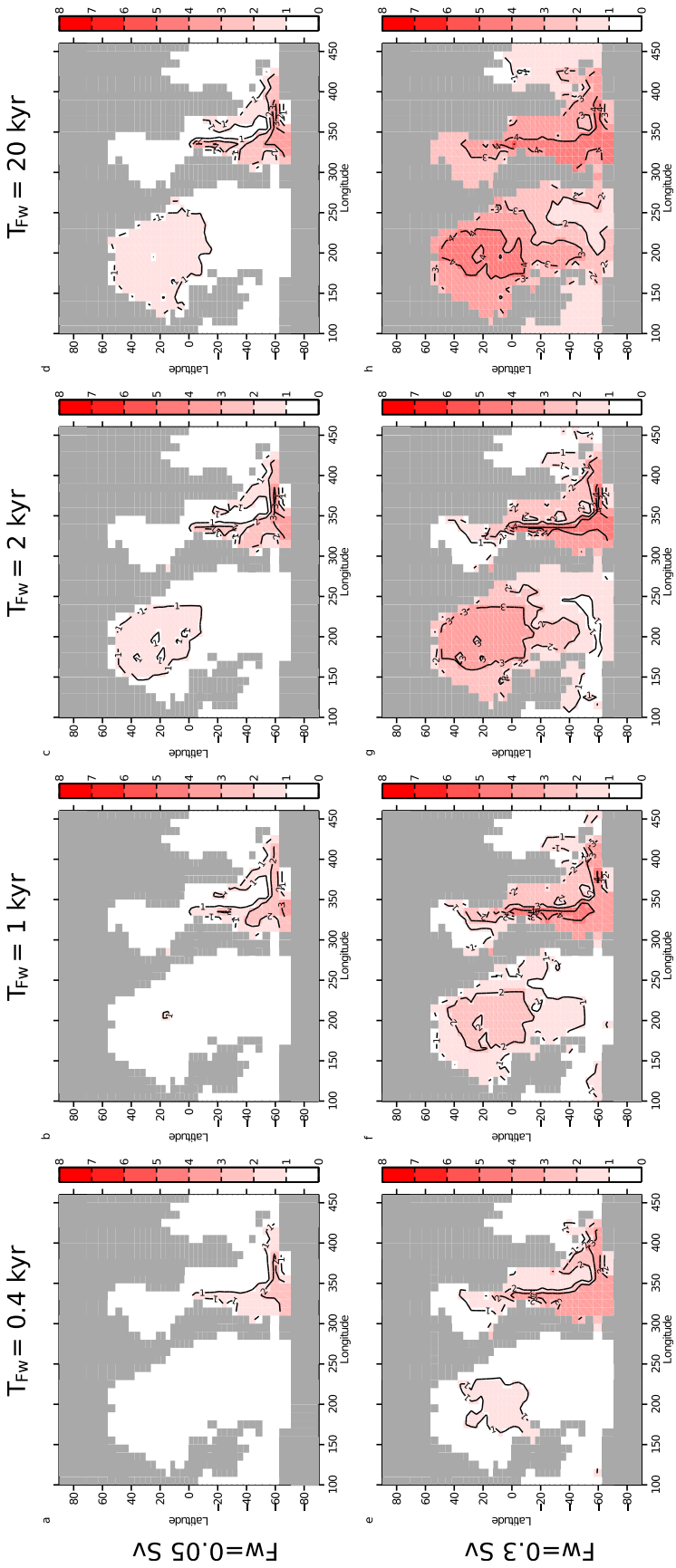

Figure 10. Global maps of $\Delta\epsilon_{Nd}$, corresponding to the absolute difference between maximum and minimum ϵ_{Nd}, at the seafloor. Results are from experiments where one single positive and negative freshwater-pulse of periods T_{Fw} = (a, e) 0.4, (b, f) 1, (c, g) 2, and (d, h) 20 kyr and amplitudes Fw = 0.05 and 0.3 *Sv* (Figures 10a–10d and 10e–10h, respectively) was applied to the Ross and Weddell Sea areas of the model (indicated as light grey areas in Figure 4b).

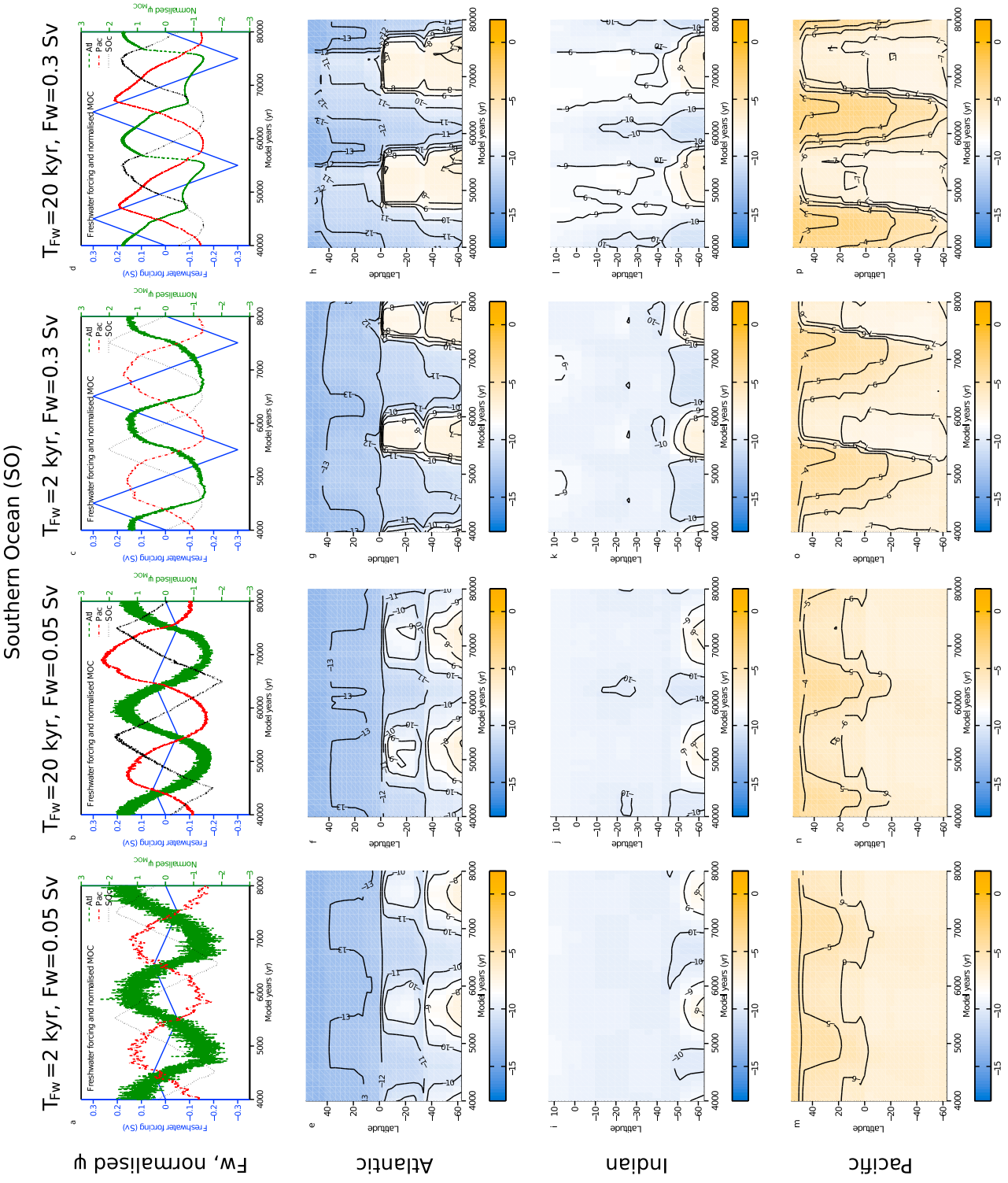
Southern Ocean (SO)
T_Fw=2 kyr, Fw=0.05 Sv
T_Fw=20 kyr, Fw=0.05 Sv
T_Fw=2 kyr, Fw=0.3 Sv
T_Fw=20 kyr, Fw=0.3 Sv
Fw, normalised ψ
Atlantic
Indian
Pacific
Freshwater forcing and normalised MOC
Atl
Pac
SOc
Freshwater forcing (Sv)
Normalised ψ_MOC
Model years (yr)
Latitude

Figure 11

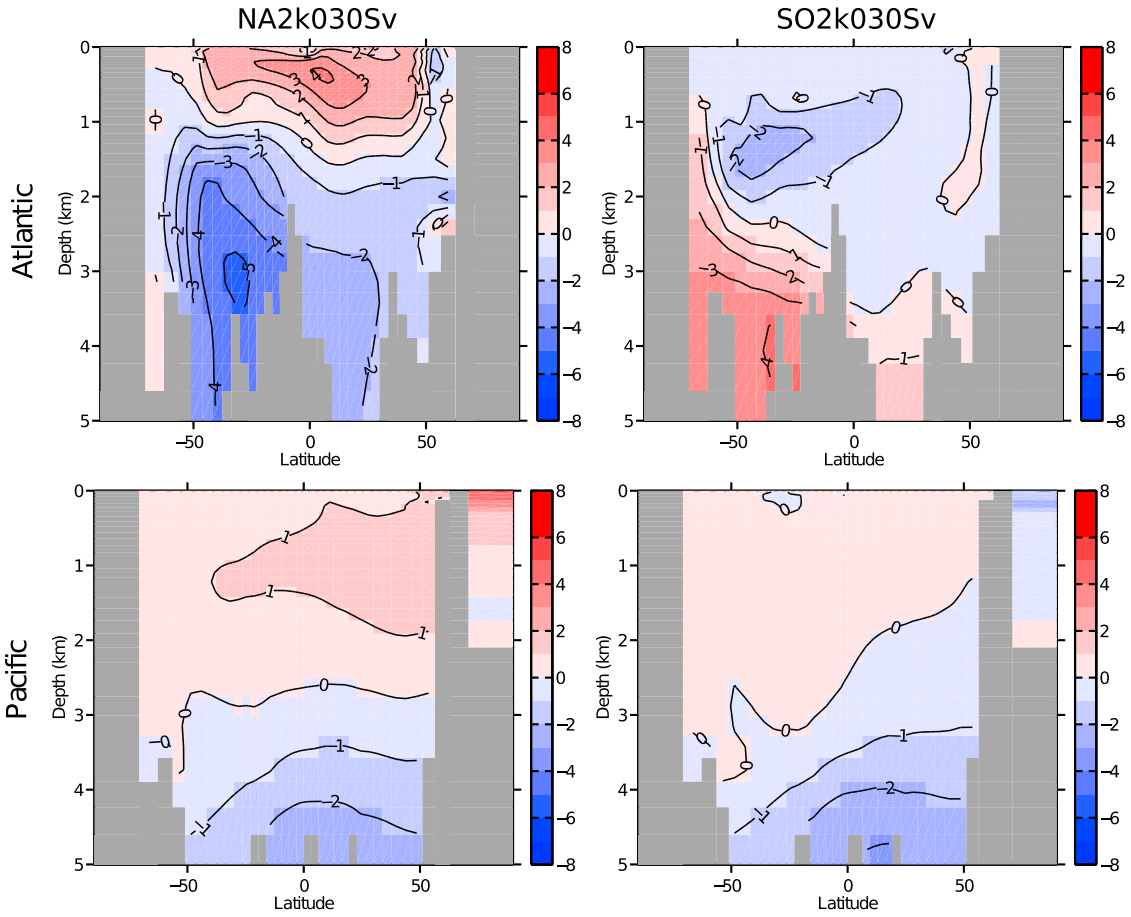

Figure 12. Vertical sections indicating differences in ϵ_{Nd} at times of most positive and most negative ϵ_{Nd} (related to on-off-states) in (a, c) NA and (b, d) SO experiments throughout the (top) central Atlantic (30–40°W) and (bottom) Pacific (150–160°W). Differences in ϵ_{Nd} are calculated between model years 6500 and 5600 (Figure 12a), 6300 and 7500 (Figure 12b), 5200 and 5900 (Figure 12c), and 5200 and 5700 (Figure 12d) (referring to Figures 8g, 8o, 11g, and 11o). Note that variations in ϵ_{Nd} hardly differ between individual periods of variations in ψ_{AMOC} and ψ_{SOMOC}.

Figure 11. (a–d) Freshwater forcing (*Sv*) and resulting normalized changes in ψ_{AMOC}, ψ_{PMOC}, ψ_{SOMOC}. In case of ψ_{SOMOC} absolute values have been calculated before normalization. Hovmöller plots indicating the temporal evolution of ϵ_{Nd} along the western boundary of (e–h) the Atlantic and (i–l) the Indian as well as through (m–p) the central Pacific. Courses of Atlantic, Indian and Pacific tracks are indicated in Figure 4, the area where freshwater-fluxes are applied is indicated in light grey in Figure 4b. Results are from experiments where freshwater fluxes of different amplitudes (Fw = 0.05 *Sv* (first and third columns) and Fw = 0.3 *Sv* (second and fourth columns)) and periods (T_{Fw} = 2 kyr (first and third columns) and T_{Fw} = 20 kyr (second and fourth columns)) are applied to the Ross and Weddell Sea areas of the model. Areas where freshwater-fluxes are applied are indicated in light grey in Figure 4b.

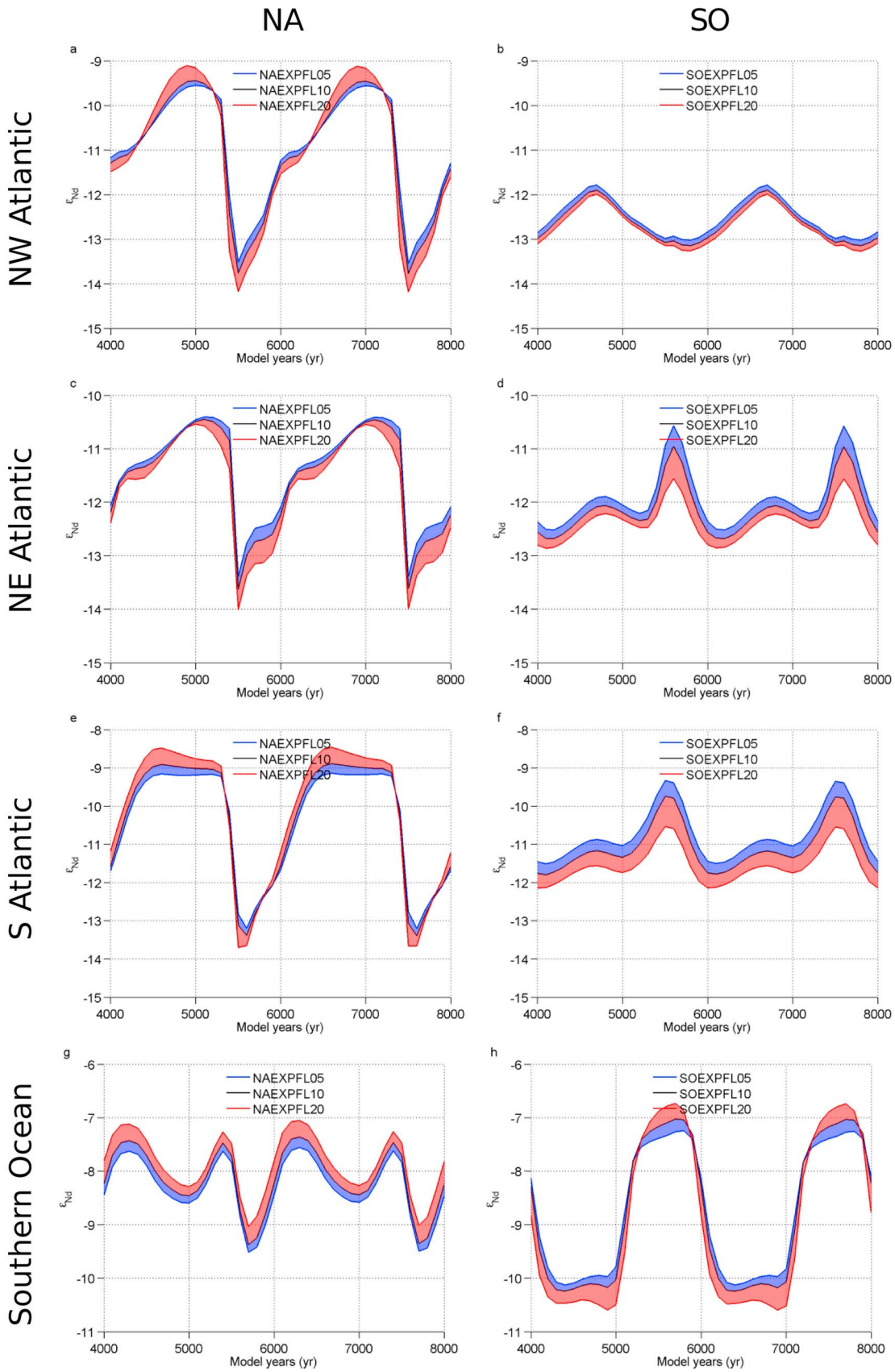
NA
SO
NW Atlantic
NE Atlantic
S Atlantic
Southern Ocean
a
b
c
d
e
f
g
h
NAEXPFL05
NAEXPFL10
NAEXPFL20
SOEXPFL05
SOEXPFL10
SOEXPFL20
Model years (yr)
4000
5000
6000
7000
8000

Figure 13

and ψ_{SOMOC}, particularly at sites in the North East Atlantic, the South Atlantic, and the Southern Ocean (Figures 14d, 14h, 14l, and 14p). In general, ϵ_{Nd} is more positive for strong ψ_{SOMOC} and more negative for weak ψ_{SOMOC}. Note however, that the relationship between ψ_{SOMOC} and ϵ_{Nd} does not hold for the entire range of ψ_{SOMOC} in the Southern Ocean. I.e., the relationship is not anymore unequivocal for ψ_{SOMOC} stronger than about 30 *Sv*.

[49] Although variations in ψ_{AMOC}, ψ_{SOMOC} and in ϵ_{Nd} are less pronounced in experiments where Fw = 0.05 *Sv* overall results are similar.

6.2. Discriminating Between Northern and Southern Origin of Changes in Water Mass Distribution

[50] In Figures 7 and 10 we have shown that the magnitude of $\Delta\epsilon_{Nd}$ depends on the magnitude and duration of changes in the overturning circulation to a certain extent. However, it also becomes clear that the global pattern of $\Delta\epsilon_{Nd}$ depends on the origin of changes in water mass distribution. In NA experiments, ϵ_{Nd} is affected most along the western boundary of the Atlantic, i.e. along the flow path of NADW, and in the South Atlantic (Figure 7). In contrast, in SO experiments, ϵ_{Nd} is particularly affected in the Atlantic sector of the Southern Ocean, i.e. close to the location where AABW is formed (Figure 10). Besides, changes in ϵ_{Nd} are more pronounced at the eastern boundary of the North Atlantic than in the western part (Figures 10a–10g, 14d, and 14h). Hence it appears that information on the origin of changes in water mass distribution can be inferred from Atlantic patterns of $\Delta\epsilon_{Nd}$. While $\Delta\epsilon_{Nd}$ is largest along the western boundary as well as in the South Atlantic in NA experiments, in SO experiments $\Delta\epsilon_{Nd}$ is largest in the Southern Ocean, the South Atlantic as well as in the Northeast Atlantic. Locations in the South Atlantic are sensitive in general. However, from experiments presented in this study it appears that it is not possible to determine whether changes in ϵ_{Nd} are either due to northern or southern changes or both based on locations in the South Atlantic alone. For this purpose additional information is required from the eastern and the western North Atlantic or the Southern Ocean.

[51] In addition, Figures 5g and 5h as well as Figures 8 and 11 show that changes in ϵ_{Nd} differ between NA and SO experiments on even larger scales. On the one hand, weaker/stronger AMOC in NA experiments leads to more positive/negative ϵ_{Nd} on a global scale. On the other hand, weaker/stronger SOMOC in SO experiments causes a shift to more positive/negative ϵ_{Nd} in the Pacific and to more negative/positive ϵ_{Nd} in the Atlantic. I.e., changes in the Atlantic and the Pacific are equal in NA experiments but are of opposite direction in SO experiments.

[52] According to our results, a discrimination between northern and southern origin of changes in ocean circulation is therefore possible based on reconstructions of ϵ_{Nd} from different sites (locations of these sites are indicated in Figure 4). First, the extent to which changes in ϵ_{Nd} can be observed in cores from the eastern and western margin of the North Atlantic or the Atlantic sector of the Southern Ocean identifies which water masses are subject to changes. I.e., if ϵ_{Nd} at the northeastern margin of the Atlantic shows variations in phase with the South Atlantic but ϵ_{Nd} at the northwestern margin does not, changes in southern source water dominate over changes in northern source water. On the other hand, if similar variations are observed at the northeastern as well as at the northwestern margins, changes in both northern source water as well as in southern source water are a likely reason. Second, if ϵ_{Nd} in the Atlantic and the central Pacific vary in phase, changes in ψ_{AMOC} are a likely cause. On the other hand, if variations in ϵ_{Nd} in the North Atlantic and the Pacific are in opposite direction, this is probably due to changes in ψ_{SOMOC}. Note however, that according to Figures 5g and 5h dating accuracy needs to be within a few hundred years for a reliable interpretation of the contrariwise behavior of ϵ_{Nd} in the Atlantic and the Pacific.

7. Discussion and Summary

[53] By analyzing results from numerous model simulations this study systematically examines the effect of changes in meridional overturning circulation on ϵ_{Nd} for the first time. Four main results of this study are briefly mentioned here and discussed in more detail thereafter: First, variations in ϵ_{Nd} of up to 5 ϵ_{Nd}-units result from periodic weakening and strengthening of the formation of NADW and AABW in millennial-scale freshwater experiments. Changes in ϵ_{Nd} of the North Atlantic or Southern Ocean end-members are relatively small, and variations in ϵ_{Nd}, e.g., in the South Atlantic thus closely reflect provenance of northern and southern source water, respectively. Second, although at first sight the magnitude of variations in ϵ_{Nd} depends on the magnitude of changes in Atlantic meridional overturning strength, no unequivocal relationship is found between ϵ_{Nd} and the formation of NADW. The relationship between ϵ_{Nd} and the formation of AABW is more pronounced. Third, the sign of changes in the Atlantic and Pacific basins as well as Atlantic patterns of $\Delta\epsilon_{Nd}$ differ between NA and SO experiments. Therefore, inferences on the origin of changes (NADW versus AABW) are possible based on the sign of the response in the Atlantic and the Pacific as well as based on the pattern of $\Delta\epsilon_{Nd}$ in the Atlantic. Fourth, absolute values of ϵ_{Nd} are affected by variations in the magnitude of particle export fluxes to a certain extent due to the associated changes in the sink of Nd and thus τ_{Nd}. However, the pattern of variations in ϵ_{Nd} caused by variations in overturning strength is hardly affected.

Figure 13. Time series of ϵ_{Nd} at sites indicated in Figure 4b: (a, b) Northwest Atlantic, (c, d) Northeast Atlantic, (e, f) the South Atlantic, and (g, h) the Southern Ocean. Results are from experiments where positive and negative freshwater fluxes of amplitude Fw = 0.3 *Sv* and of period T_{Fw} = 2 kyr are applied to (left) the North Atlantic (corresponding to experiment NA2k030Sv) and (right) the Ross and Weddell Sea areas of the model (corresponding to experiment SO2k030Sv). CTRL particle export fluxes of POC, $CaCO_3$ and opal are scaled in the North Atlantic (NA) or the Southern Ocean (SO) by factors 1/2, 1, and 2 and are kept constant at these levels throughout the corresponding simulation. Shaded areas indicate the range within which ϵ_{Nd} varies in cases where particle-types are scaled individually.

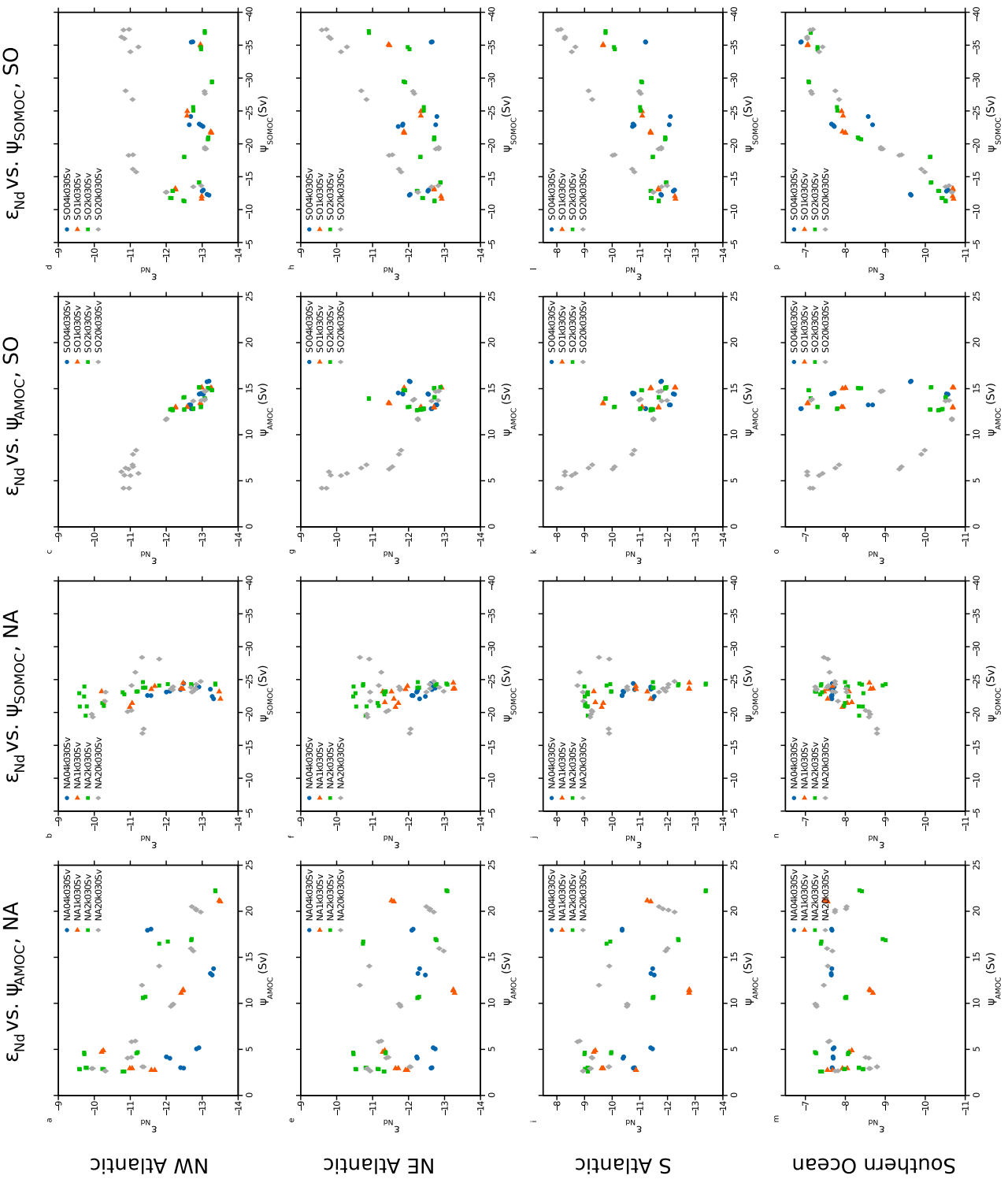
εNd vs. ΨAMOC, NA
εNd vs. ΨSOMOC, NA
εNd vs. ΨAMOC, SO
εNd vs. ΨSOMOC, SO
NW Atlantic
NE Atlantic
S Atlantic
Southern Ocean
NA04k030Sv
NA1k030Sv
NA2k030Sv
NA20k030Sv
SO04k030Sv
SO1k030Sv
SO2k030Sv
SO20k030Sv
ΨAMOC (Sv)
ΨSOMOC (Sv)
εNd

Figure 14

[54] Overall, our results indicate that in experiments where millennial-scale variations are applied to the overturning circulation and thus to the distribution of water masses, variations in ϵ_{Nd} closely reflect these variations. Furthermore, in our experiments changes in ϵ_{Nd} of end-members are much smaller than variations in ϵ_{Nd} due to changes in water mass distribution. Note however, that this does not allow to exclude changes in end-member composition on glacial-interglacial time-scales (as reported by *Gutjahr et al.* [2008] and *Arsouze et al.* [2008]).

[55] Neither the pattern, nor the magnitude of $\Delta\epsilon_{Nd}$, and thus the sensitivity of ϵ_{Nd} to changes in overturning strength, are globally uniform. Sites where records of ϵ_{Nd} shall be extracted from the sediments hence need to be chosen with care. In general, largest variations in ϵ_{Nd} are found at locations where the mix of major water masses varies depending on the circulation regime. In seeking maximum response in ϵ_{Nd}, paleoceanographic studies should therefore focus on such regions.

[56] More specifically, ϵ_{Nd} is sensitive to changes in AMOC, particularly in the South Atlantic, where Atlantic main water masses, NADW and AABW, prevail depending on pattern and strength of the AMOC. ϵ_{Nd} is more negative during periods of strong formation of NADW and more positive during periods when formation of NADW is weak. At the same time ϵ_{Nd} is more positive if formation of AABW is strong and more negative if formation of SOMOC is weak. Therefore, variations in ϵ_{Nd}, e.g., in the South Atlantic do not simply reflect increasing/decreasing strength of NADW, but also an increasing/decreasing strength of AABW or a combination of changes in NADW and AABW, respectively. This is in general agreement with the interpretation of *Piotrowski et al.* [2004, 2005, 2008] and indicates that it is not possible to infer on the origin of changes based on one single core from the South Atlantic, without further constraints from other proxies such as $\delta^{13}C$ (comparable to *Piotrowski et al.* [2008, 2009]) which in turn introduce additional uncertainties. Though, to infer on the origin of changes in the AMOC is of interest with regard to changes on millennial [*Weaver et al.*, 2003; *Piotrowski et al.*, 2004; *Gutjahr et al.*, 2010] as well as on orbital time-scales [*Lynch-Stieglitz et al.*, 2007; *Piotrowski et al.*, 2008]. Our results indicate that constraining the origin of changes in AMOC is possible based on the pattern of $\Delta\epsilon_{Nd}$ in the northwest and the northeast Atlantic as well as in the Southern Ocean. However, as these differences occur on relatively small, i.e., sub basin scale and as our model is only coarsely resolved, confidence into these results should be enhanced by models with higher resolution. Further large-scale differences in the temporal evolution of ϵ_{Nd} in the Atlantic and the Pacific can be observed in our NA and SO experiments, thus providing additional constraints on the origin of changes in AMOC. Note, that in this regard limitations could result from dating accuracy which is required to be within the range of a few hundred years.

[57] On the one hand, in our freshwater experiments we find the magnitude of variations in ϵ_{Nd} ($\Delta\epsilon_{Nd}$) to depend on the magnitude and the duration of changes in strength of the overturning circulation, thus indicating that $\Delta\epsilon_{Nd}$ yields information about the magnitude of changes, e.g., in the rate of the AMOC. On the other hand, scatterplots of ψ_{AMOC} and ψ_{SOMOC} versus ϵ_{Nd} show that it is difficult to derive information on the rate of the AMOC based on ϵ_{Nd}, because the relationship between ψ_{AMOC} and ϵ_{Nd} is rarely unequivocal. In contrast, the relationship is more pronounced between SOMOC and ϵ_{Nd}, between which linear relationships exist at some sites. Note however, that the relationship does not hold for the entire range of SOMOC strength (i.e., for large magnitudes), e.g., in the Southern Ocean.

[58] Scaling of particle fluxes in regions of deep-water formation affects absolute values of ϵ_{Nd} as well as the magnitude of $\Delta\epsilon_{Nd}$ to some extent but hardly affects the pattern of ϵ_{Nd}. Overall, the effect of changes in export fluxes on ϵ_{Nd} is small compared to the effect of changes in circulation strength. This indicates that changes in pattern and magnitude of export fluxes do not introduce large uncertainty in the interpretation of $\Delta\epsilon_{Nd}$ as circulation changes. It is important to note, that these results depend on the assumption of non-preferential scavenging, which is reasonable as long as no indication for preferential scavenging is found [*Arsouze et al.*, 2009; *Rempfer et al.*, 2011]. New insight into the marine Nd cycle will emerge, e.g., from the GEOTRACES program in the near future [*SCOR Working Group*, 2007].

[59] In this context we also emphasize general uncertainties associated with the nature and magnitude of sources of Nd. Recent studies indicate that ϵ_{Nd} is modified at continental margins and young volcanic arcs and that continental margins and the seafloor could act as sources of Nd [*van de Flierdt et al.*, 2004; *Lacan and Jeandel*, 2005a; *Johannesson and Burdige*, 2007; *Rickli et al.*, 2010; *Horikawa et al.*, 2010; *Carter et al.*, 2012; *Stichel et al.*, 2012]. This means that ϵ_{Nd} of any water mass not only depends on the isotopic signature of the two main end-members North Atlantic and North Pacific. Our simplified approach takes this into account by assuming a globally homogeneous boundary source and is a reasonable first order approach considering its success in simulating modern $[Nd]_d$ and ϵ_{Nd}. However, it probably does not cover the complexity associated with the boundary source and will thus prove incomplete as soon as more detailed insight is gained into the nature of this source (e.g., through the GEOTRACES program) [*SCOR Working Group*, 2007].

Figure 14. (a, c, e, g, i, k, m, o) Scatterplots of ψ_{AMOC} versus ϵ_{Nd} and (b, d, f, h, j, l, n, p) ψ_{SOMOC} versus ϵ_{Nd} for NA and SO experiments. Note the direction of x-axes that indicate ψ_{SOMOC} is reverse. Colors indicate different freshwater experiments and are specified on the panels (see Table 2 for further details). Results are from Blake Ridge, Northwest Atlantic (Figures 14a–14d), Northeast Atlantic (Figures 14e–14h), South Atlantic (Figures 14i–14l), and Southern Ocean (Figures 14m–14p). The location of each site is indicated in Figure 4b.

[60] In conclusion, our millennial-scale freshwater experiments indicate the large potential of ϵ_{Nd} as a paleocirculation tracer but also indicate the limitations of quantitative reconstructions of changes in the Atlantic Meridional Overturning Circulation.

[61] **Acknowledgments.** This work was funded through the Marie Curie Research Training Network NICE (Network for Ice sheet and Climate Evolution). Support by the European Project on Ocean Acidification (EPOCA, FP7/2007–2013; 211384), Past4Future (grant 243908), the EU FP7 project CARBOCHANGE (grant agreement 264879), and the Swiss National Science Foundation are acknowledged. Thanks are due to S. Ritz for the development of the coupled Bern3D code as well as for stimulating discussions. We are also grateful to two anonymous reviewers, whose valuable comments led to significant improvements in the manuscript.

References

Albarède, F., and S. L. Goldstein (1992), World map of Nd isotopes in sea-floor ferromanganese deposits, *Geology*, *20*, 761–763.

Albarède, F., S. L. Goldstein, and D. Dautel (1997), The neodymium isotopic composition of manganese nodules from the Southern and Indian oceans, the global oceanic neodymium budget, and their bearing on deep ocean circulation, *Geochim. Cosmochim. Acta*, *61*, 1277–1291.

Amakawa, H., D. S. Alibo, and Y. Nozaki (2000), Nd isotopic composition and REE pattern in the surface waters of the eastern Indian Ocean and its adjacent seas, *Geochim. Cosmochim. Acta*, *64*, 1715–1727.

Amakawa, H., Y. Nozaki, D. S. Alibo, J. Zhang, K. Fukugawa, and H. Nagai (2004), Neodymium isotopic variations in Northwest Pacific waters, *Geochim. Cosmochim. Acta*, *68*, 715–727.

Amakawa, H., K. Sasaki, and M. Ebihara (2009), Nd isotopic composition in the central North Pacific, *Geochim. Cosmochim. Acta*, *73*, 4705–4719.

Andersson, P. S., D. Porcelli, M. Frank, G. Björk, R. Dahlqvist, and O. Gustafsson (2008), Neodymium isotopes in seawater from the Barents Sea and Fram Strait Arctic-Atlantic gateways, *Geochim. Cosmochim. Acta*, *72*, 2854–2867.

Arsouze, T., J. C. Dutay, F. Lacan, and C. Jeandel (2007), Modeling the neodymium isotopic composition with a global ocean circulation model, *Chem. Geol.*, *239*, 165–177.

Arsouze, T., J.-C. Dutay, M. Kageyama, F. Lacan, R. Alkama, O. Marti, and C. Jeandel (2008), A modeling sensitivity study of the influence of the Atlantic meridional overturning circulation on neodymium isotopic composition at the Last Glacial Maximum, *Clim. Past*, *4*, 191–203.

Arsouze, T., J.-C. Dutay, F. Lacan, and C. Jeandel (2009), Reconstructing the Nd oceanic cycle using a coupled dynamical biogeochemical model, *Biogeosciences*, *6*, 2829–2846.

Bertram, C., and H. Elderfield (1993), The geochemical balance of the rare earth elements and neodymium isotopes in the oceans, *Geochim. Cosmochim. Acta*, *57*, 1957–1986.

Burton, K. W., and D. Vance (2000), Glacial-interglacial variations in the neodymium isotope composition of seawater in the Bay of Bengal recorded by planktonic foraminifera, *Earth Planet. Sci. Lett.*, *176*, 425–441.

Carter, P., D. Vance, C. Hillenbrand, J. Smith, and D. Shoosmith (2012), The neodymium isotopic composition of waters masses in the eastern Pacific Sector of the Southern Ocean, *Geochim. Cosmochim. Acta*, *79*, 41–59.

Dahlqvist, R., P. Andersson, and J. Ingri (2005), The concentration and isotopic composition of diffusible Nd in fresh and marine waters, *Earth Planet. Sci. Lett.*, *233*, 9–16.

Edwards, N., and R. Marsh (2005), Uncertainties due to transport-parameter sensitivity in an efficient 3-D ocean-climate model, *Clim. Dyn.*, *24*, 415–433.

Elderfield, H., and M. J. Greaves (1982), The rare earth elements in seawater, *Nature*, *296*, 214–219.

Elmore, A. C., A. M. Piotrowski, J. D. Wright, and A. E. Scrivner (2011), Testing the extraction of past seawater Nd isotopic composition from North Atlantic deep sea sediments and foraminifera, *Geochem. Geophys. Geosyst.*, *12*, Q09008, doi:10.1029/2011GC003741.

Foster, G. L., D. Vance, and J. Prytulak (2007), No change in the neodymium isotope composition of deep water exported from the North Atlantic on glacial-interglacial time scales, *Geology*, *35*, 37–40.

Frank, M. (2002), Radiogenic isotopes: Tracers of past ocean circulation and erosional input, *Rev. Geophys.*, *40*(1), 1001, doi:10.1029/2000RG000094.

Ganachaud, A., and C. Wunsch (2000), Improved estimates of global ocean circulation, heat transport and mixing from hydrographic data, *Nature*, *408*, 453–457.

Godfrey, L. V., B. Zimmermann, D. C. Lee, R. L. King, J. D. Vervoort, R. M. Sherrell, and A. N. Halliday (2009), Hafnium and neodymium isotope variations in NE Atlantic seawater, *Geochem. Geophys. Geosyst.*, *10*, Q08015, doi:10.1029/2009GC002508.

Goldstein, S. J., and S. B. Jacobsen (1987), The Nd and Sr isotopic systematics of river-water dissolved material: Implications for the sources of Nd and Sr in seawater, *Chem. Geol.*, *66*, 245–272.

Goldstein, S. L., and S. Hemming (2003), Long-lived isotopic tracers in oceanography, paleoceanography, and ice-sheet dynamics, in *Treatise on Geochemistry*, vol. 6, *The Oceans and Marine Geochemistry*, edited by H. D. Holland and K. K. Turekian, pp. 453–489, Elsevier, Oxford, U. K.

Greaves, M., H. Elderfield, and E. Sholkovitz (1999), Aeolian sources of rare earth elements to the Western Pacific Ocean, *Mar. Chem.*, *68*, 31–38.

Gutjahr, M., and J. Lippold (2011), Early arrival of Southern Source Water in the deep North Atlantic prior to Heinrich event 2, *Paleoceanography*, *26*, PA2101, doi:10.1029/2011PA002114.

Gutjahr, M., M. Frank, C. Stirling, L. Keigwin, and A. Halliday (2008), Tracing the Nd isotope evolution of North Atlantic Deep and Intermediate Waters in the western North Atlantic since the Last Glacial Maximum from Blake Ridge sediments, *Earth Planet. Sci. Lett.*, *266*, 61–77.

Gutjahr, M., B. A. A. Hoogakker, M. Frank, and I. N. McCave (2010), Changes in North Atlantic Deep Water strength and bottom water masses during Marine Isotope Stage 3 (45–35 ka BP), *Quat. Sci. Rev.*, *29*, 2451–2461.

Henry, F., C. Jeandel, B. Dupre, and J. Minster (1994), Particulate and dissolved Nd in the Western Mediterranean Sea: sources, fates and budget, *Mar. Chem.*, *45*, 283–305.

Hesse, T., M. Butzin, T. Bickert, and G. Lohmann (2011), A model-data comparison of δ^{13}C in the glacial Atlantic Ocean, *Paleoceanography*, *26*, PA3220, doi:10.1029/2010PA002085.

Horikawa, K., Y. Asahara, K. Yamamoto, and Y. Okazaki (2010), Intermediate water formation in the Bering Sea during glacial periods: Evidence from neodymium isotope ratios, *Geology*, *38*, 435–438.

Jacobsen, S. B., and G. Wasserburg (1980), Sm-Nd isotopic evolution of chondrites, *Earth Planet. Sci. Lett.*, *50*, 139–155.

Jeandel, C. (1993), Concentration and isotopic composition of Nd in the South Atlantic Ocean, *Earth Planet. Sci. Lett.*, *117*, 581–591.

Jeandel, C., J. K. Bishop, and A. Zindler (1995), Exchange of neodymium and its isotopes between seawater and small and large particles in the Sargasso Sea, *Geochim. Cosmochim. Acta*, *59*, 535–547.

Jeandel, C., D. Thouron, and M. Fieux (1998), Concentrations and isotopic compositions of neodymium in the eastern Indian Ocean and Indonesian straits, *Geochim. Cosmochim. Acta*, *62*, 2597–2607.

Johannesson, K. H., and D. J. Burdige (2007), Balancing the global oceanic neodymium budget: Evaluating the role of groundwater, *Earth Planet. Sci. Lett.*, *253*, 129–142.

Keigwin, L. D., and E. A. Boyle (2008), Did North Atlantic overturning halt 17,000 years ago?, *Paleoceanography*, *23*, PA1101, doi:10.1029/2007PA001500.

Klevenz, V., D. Vance, D. N. Schmidt, and K. Mezger (2008), Neodymium isotopes in benthic foraminifera: Core-top systematics and a down-core record from the Neogene south Atlantic, *Earth Planet. Sci. Lett.*, *265*, 571–587.

Lacan, F., and C. Jeandel (2001), Tracing Papua New Guinea imprint on the central Equatorial Pacific Ocean using neodymium isotopic compositions and Rare Earth Element patterns, *Earth Planet. Sci. Lett.*, *186*, 497–512.

Lacan, F., and C. Jeandel (2004a), Denmark Strait water circulation traced by heterogeneity in neodymium isotopic compositions, *Deep Sea Res., Part I*, *51*, 71–82.

Lacan, F., and C. Jeandel (2004b), Neodymium isotopic composition and rare earth element concentration in the deep and intermediate Nordic Seas: Constraints on the Iceland Scotland Overflow Water signature, *Geochem. Geophys. Geosyst.*, *5*, Q11006, doi:10.1029/2004GC000742.

Lacan, F., and C. Jeandel (2004c), Subpolar Mode Water formation traced by neodymium isotopic composition, *Geophys. Res. Lett.*, *31*, L14306, doi:10.1029/2004GL019747.

Lacan, F., and C. Jeandel (2005a), Neodymium isotopes as a new tool for quantifying exchange fluxes at the continent-ocean interface, *Earth Planet. Sci. Lett.*, *232*, 245–257.

Lacan, F., and C. Jeandel (2005b), Acquisition of the neodymium isotopic composition of the North Atlantic Deep Water, *Geochem. Geophys. Geosyst.*, *6*, Q12008, doi:10.1029/2005GC000956.

Lippold, J., J. Grützner, D. Winter, Y. Lahaye, A. Mangini, and M. Christl (2009), Does sedimentary ^{231}Pa/^{230}Th from the Bermuda Rise monitor past Atlantic Meridional Overturning Circulation?, *Geophys. Res. Lett.*, *36*, L12601, doi:10.1029/2009GL038068.

Lynch-Stieglitz, J. (2003), Tracers of past ocean circulation, in *Treatise on Geochemistry*, vol. 6, *The Oceans and Marine Geochemistry*, edited by H. D. Holland and K. K. Turekian, pp. 433–451, Elsevier, Oxford U. K.

Lynch-Stieglitz, J., et al. (2007), Atlantic meridional overturning circulation during the Last Glacial Maximum, *Science*, *316*, 66–69.

Marchal, O., and W. B. Curry (2008), On the abyssal circulation in the glacial Atlantic, *J. Phys. Oceanogr.*, *38*, 2014–2037.

Marchal, O., T. Stocker, and F. Joos (1998), Impact of oceanic reorganizations on the ocean carbon cycle and atmospheric carbon dioxide content, *Paleoceanography*, *13*, 225–244.

Martin, E., and B. Haley (2000), Fossil fish teeth as proxies for seawater Sr and Nd isotopes, *Geochim. Cosmochim. Acta*, *64*, 835–847.

Müller, S. A., F. Joos, N. R. Edwards, and T. F. Stocker (2006), Water mass distribution and ventilation time scales in a cost-efficient, three-dimensional ocean model, *J. Clim.*, *19*, 5479–5499.

Parekh, P., F. Joos, and S. A. Müller (2008), A modeling assessment of the interplay between aeolian iron fluxes and iron-binding ligands in controlling carbon dioxide fluctuations during Antarctic warm events, *Paleoceanography*, *23*, PA4202, doi:10.1029/2007PA001531.

Piepgras, D. J., and S. B. Jacobsen (1988), The isotopic composition of neodymium in the North Pacific, *Geochim. Cosmochim. Acta*, *52*, 1373–1381.

Piepgras, D. J., and G. J. Wasserburg (1980), Neodymium isotopic variations in seawater, *Earth Planet. Sci. Lett.*, *50*, 128–138.

Piepgras, D. J., and G. J. Wasserburg (1982), Isotopic composition of neodymium in waters from the Drake Passage, *Science*, *217*, 207–214.

Piepgras, D. J., and G. J. Wasserburg (1983), Influence of the Mediterranean Outflow on the isotopic composition of neodymiumin waters of the North-Atlantic, *J. Geophys. Res.*, *88*, 5997–6006.

Piepgras, D. J., and G. Wasserburg (1987), Rare earth element transport in the western North Atlantic inferred from Nd isotopic observations, *Geochim. Cosmochim. Acta*, *51*, 1257–1271.

Piepgras, D. J., G. Wasserburg, and E. Dasch (1979), The isotopic composition of Nd in different ocean masses, *Earth Planet. Sci. Lett.*, *45*, 223–236.

Piotrowski, A. M., S. L. Goldstein, S. R. Hemming, and R. G. Fairbanks (2004), Intensification and variability of ocean thermohaline circulation through the last deglaciation, *Earth Planet. Sci. Lett.*, *225*, 205–220.

Piotrowski, A. M., S. L. Goldstein, S. R. Hemming, and R. G. Fairbanks (2005), Temporal relationships of carbon cycling and ocean circulation at glacial boundaries, *Science*, *307*, 1933–1938.

Piotrowski, A. M., S. L. Goldstein, S. R., Hemming, R. G. Fairbanks, and D. R. Zylberberg (2008), Oscillating glacial northern and southern deep water formation from combined neodymium and carbon isotopes, *Earth Planet. Sci. Lett.*, *272*, 394–405.

Piotrowski, A. M., V. K. Banakar, A. E. Scrivner, H. Elderfield, A. Galy, and A. Dennis (2009), Indian Ocean circulation and productivity during the last glacial cycle, *Earth Planet. Sci. Lett.*, *285*, 179–189.

Porcelli, D., P. S. Andersson, M. Baskaran, M. Frank, G. Björk, and I. Semiletov (2009), The distribution of neodymium isotopes in Arctic Ocean basins, *Geochim. Cosmochim. Acta*, *73*, 2645–2659.

Rempfer, J., T. F. Stocker, F. Joos, J.-C. Dutay, and M. Siddall (2011), Modelling Nd-isotopes with a coarse resolution ocean circulation model: Sensitivities to model parameters and source/sink distributions, *Geochim. Cosmochim. Acta*, *75*, 5927–5950.

Rickli, J., M. Frank, and A. N. Halliday (2009), The hafnium–neodymium isotopic composition of Atlantic seawater, *Earth Planet. Sci. Lett.*, *280*, 118–127.

Rickli, J., M. Frank, A. R. Baker, S. Aciego, G. de Souza, R. B. Georg, and A. N. Halliday (2010), Hafnium and neodymium isotopes in surface waters of the eastern Atlantic Ocean: Implications for sources and inputs of trace metals to the ocean, *Geochim. Cosmochim. Acta*, *74*, 540–557.

Ritz, S. P., T. F. Stocker, and F. Joos (2011a), A coupled dynamical ocean energy balance atmosphere model for paleoclimate studies, *J. Clim.*, *24*, 349–375.

Ritz, S. P., T. F. Stocker, and J. P. Severinghaus (2011b), Noble gases as proxies of mean ocean temperature: Sensitivity studies using a climate model of reduced complexity, *Quat. Sci. Rev.*, *30*, 3728–3741.

Roberts, N. L., A. M. Piotrowski, J. F. McManus, and L. D. Keigwin (2010), Synchronous deglacial overturning and water mass source changes, *Science*, *327*, 75–78.

Robinson, L., and T. van de Flierdt (2009), Southern Ocean evidence for reduced export of North Atlantic Deep Water during Heinrich event 1, *Geology*, *37*, 195–198.

Rutberg, R. L., S. R. Hemming, and S. L. Goldstein (2000), Reduced North Atlantic Deep Water flux to the glacial Southern Ocean inferred from neodymium isotope ratios, *Nature*, *405*, 935–938.

Sarmiento, J. L., and N. Gruber (2006), *Ocean Biogeochemical Dynamics*, Princeton Univ. Press, Princeton, N. J.

Schmittner, A. (2005), Decline of the marine ecosystem caused by a reduction in the Atlantic overturning circulation, *Nature*, *434*, 628–633.

SCOR Working Group (2007), GEOTRACES - An international study of the global marine biogeochemical cycles of trace elements and their isotopes, *Chem. Erde*, *67*, 85–131.

Shimizu, H., K. Tachikawa, A. Masuda, and Y. Nozaki (1994), Cerium and neodymium isotope ratios and REE patterns in seawater from the North Pacific Ocean, *Geochim. Cosmochim. Acta*, *58*, 323–333.

Siddall, M., T. F. Stocker, G. M. Henderson, F. Joos, M. Frank, N. R. Edwards, S. P. Ritz, and S. A. Müller (2007), Modeling the relationship between $^{231}Pa/^{230}Th$ distribution in North Atlantic sediment and Atlantic meridional overturning circulation, *Paleoceanography*, *22*, PA2214, doi:10.1029/2006PA001358.

Siddall, M., S. Khatiwala, T. van de Flierdt, K. Jones, S. L. Goldstein, S. R. Hemming, and R. F. Anderson (2008), Towards explaining the Nd paradox using reversible scavenging in an ocean general circulation model, *Earth Planet. Sci. Lett.*, *274*, 448–461.

Spivack, A., and G. Wasserburg (1988), Neodymium isotopic composition of the Mediterranean outflow and the eastern North Atlantic, *Geochim. Cosmochim. Acta*, *52*, 2762–2773.

Stichel, T., M. Frank, J. Rickli, and B. A. Haley (2012), The hafnium and neodymium isotope composition of seawater in the Atlantic sector of the Southern Ocean, *Earth Planet. Sci. Lett.*, *317–318*, 282–294.

Stordal, M., and G. Wasserburg (1986), Neodymium isotopic study of Baffin Bay water: sources of REE from very old terranes, *Earth Planet. Sci. Lett.*, *77*, 259–272.

Tachikawa, K., C. Jeandel, and M. Roy-Barman (1999), A new approach to the Nd residence time in the ocean: the role of atmospheric inputs, *Earth Planet. Sci. Lett.*, *170*, 433–446.

Tachikawa, K., V. Athias, and C. Jeandel (2003), Neodymium budget in the modern ocean and paleo-oceanographic implications, *J. Geophys. Res.*, *108*(C8), 3254, doi:10.1029/1999JC000285.

Tachikawa, K., M. Roy-Barman, A. Michard, D. Thouron, D. Yeghicheyan, and C. Jeandel (2004), Neodymium isotopes in the Mediterranean Sea: Comparison between seawater and sediment signals, *Geochim. Cosmochim. Acta*, *68*, 3095–3106.

Talley, L. D., J. L. Reid, and P. E. Robbins (2003), Data-based meridional overturning streamfunctions for the global ocean, *J. Clim.*, *16*, 3213–3226.

Tschumi, T., F. Joos, and P. Parekh (2008), How important are Southern Hemisphere wind changes for low glacial carbon dioxide? A model study, *Paleoceanography*, *23*, PA4208, doi:10.1029/2008PA001592.

van de Flierdt, T., M. Frank, D.-C. Lee, A. N. Halliday, B. C. Reynolds, and J. R. Hein (2004), New constraints on the sources and behavior of neodymium and hafnium in seawater from Pacific Ocean ferromanganese crusts, *Geochim. Cosmochim. Acta*, *68*, 3827–3843.

van de Flierdt, T., L. F. Robinson, J. F. Adkins, S. R. Hemming, and S. L. Goldstein (2006), Temporal stability of the neodymium isotope signature of the Holocene to glacial North Atlantic, *Paleoceanography*, *21*, PA4102, doi:10.1029/2006PA001294.

van de Flierdt, T., S. L. Goldstein, S. R. Hemming, M. Roy, M. Frank, and A. N. Halliday (2007), Global neodymium-hafnium isotope systematics —Revisited, *Earth Planet. Sci. Lett.*, *259*, 432–441.

van de Flierdt, T., L. F. Robinson, and J. F. Adkins (2010), Deep-sea coral aragonite as a recorder for the neodymium isotopic composition of seawater, *Geochim. Cosmochim. Acta*, *74*, 6014–6032.

Vance, D., A. E. Scrivner, P. Beney, M. Staubwasser, G. M. Henderson, and N. C. Slowey (2004), The use of foraminifera as a record of the past neodymium isotope composition of seawater, *Paleoceanography*, *19*, PA2009, doi:10.1029/2003PA000957.

von Blanckenburg, F. (1999), Paleoceanography: Tracing past ocean circulation?, *Science*, *286*, 1862–1863.

Weaver, A. J., O. A. Saenko, P. U. Clark, and J. X. Mitrovica (2003), Meltwater pulse 1A from Antarctica as a trigger of the Bølling-Allerød Warm Interval, *Science*, *299*, 1709–1713.

Yasuhara, M., T. M. Cronin, P. B. deMenocal, H. Okahashi, and B. K. Linsley (2008), Abrupt climate change and collapse of deep-sea ecosystems, *Proc. Natl. Acad. Sci.*, *105*, 1556–1560.

Zimmermann, B., D. Porcelli, M. Frank, P. Andersson, M. Baskaran, D.-C. Lee, and A. Halliday (2009a), Hafnium isotopes in Arctic Ocean water, *Geochim. Cosmochim. Acta*, *73*, 3218–3233.

Zimmermann, B., D. Porcelli, M. Frank, J. Rickli, D.-C. Lee, and A. N. Halliday (2009b), The hafnium isotope composition of Pacific Ocean water, *Geochim. Cosmochim. Acta*, *73*, 91–101.